Supporting Information

Molecular Engineering of Supramolecular Polymer Adhesive with Confined Water and a Single Crown Ether

Qiangqiang Xu,[a] Paulina Szymoniak,[b] Mohamed Aejaz Kolmangadi,[b] Zerui Yang,[a] Shixian Wang,[c],[d] Yurui Gao,[c],[d]* Jie Shang,[a] Johannes Hunger,[e] Aitkazy Kaisha,[f] Abdurakhman Aldiyarov,[g] Andreas Schönhals,[b],[h]* Yan Ge,[a]* Zhenhui Qi[a]*

[a]Sino-German Joint Research Lab for Space Biomaterials and Translational Technology, Synergetic Innovation Center of Biological Optoelectronics and Healthcare Engineering, School of Life Sciences, Northwestern Polytechnical University, Xi'an, Shaanxi 710072, P. R. China

[b]Bundesanstalt für Materialforschung und -prüfung (BAM), Unter den Eichen 87, 12205 Berlin, Germany

[c]Laboratory of Theoretical and Computational Nanoscience, National Centre for Nanoscience and Technology, Chinese Academy of Sciences, Beijing 100190, China

[d]University of Chinese Academy of Sciences, Beijing 100049, P. R. China

[e]Max Planck Institute for Polymer Research, Ackermannweg 10, 55128 Mainz, Germany

[f]Renewable Energy Laboratory, National Laboratory Astana (NLA), Nazarbayev University, Astana, Kazakhstan

[g]Al-Farabi Kazakh National University, Al-Farabi Av., 71, 050040 Almaty, Kazakhstan

[h]Institut für Chemie, Technische Universität Berlin, Straße des 17. Juni 135, 10623 Berlin, Germany

Email: qi@nwpu.edu.cn; ge@nwpu.edu.cn; gaoyr@nanoctr.cn; andreas.schoenhals@bam.de

Table of Contents

1. Material and Methods

Unless otherwise noted, all materials, reagents and solvents were from commercial suppliers and used without further purification. Compound **C7Se** and its control **C7** were kindly gifted by Metaxinmei Inc, and the detailed synthesis was followed according to our previous reported protocols. [S1]

NMR data were obtained by a Bruker Avance III-400 spectrophotometer, Jeol Eclipse 500 MHz, or Bruker AVANCE III 700 MHz NMR spectrometers. For the structural characterization of synthetic compounds, high-resolution mass spectrum (HR-MS) was performed using an electrospray ionization (ESI) interface on an Agilent LC/MSD TOF system. Fourier-transform IR (FT-IR) spectra were recorded by a Thermo Scientific Nicolet iS20 FT-IR instrument.

The thermograms of the adhesive materials were measured using differential scanning calorimetry (DSC; MDSC2910, TA Instruments). Fast scanning calorimetry was carried employing a Mettler Toledo Flash DSC1 device with using the UFS1 twin sensor chip as measuring cell having two active sensor areas. [S2] The Flash DSC1 is power compensated differential scanning calorimeter and allows for heating rates in the range from 0.5 K/s to 4×10^4 K/s. The accessible cooling rates are one order of magnitude lower. The flow rate N_2 purge gas was 40 mL/min.

Dielectric spectroscopy was carried out in a frequency range from 10^{-1} to 10^6 Hz and at temperatures between -100 and 60 °C with a high-resolution ALPHA Analyzer interfaced to an active sample head (Novocontrol, Montabaur, Germany). The measurements were carried out in parallel geometry. The temperature of the sample was controlled by a Quatro Novocontrol cryo-system with a stability of 0.1 K using nitrogen as heating agent. To avoid the evaporation of water during the measurements, a custom made hermetically sealed dielectric cell was used for the measurement. For details see ref S3.

The thermogravimetric analysis (TGA) was carried out using a Netzsch Instruments STA 449 F3 Jupiter analyzer with an automated vertical overhead thermobalance. The samples were scanned from room temperature to 600 °C at a rate of 10.0 K/min in flowing nitrogen. The adhesion strength measurements were performed on a pull-off adhesion tester (HY-0580) with a pull rate of 100 mm/s. The fluorescent images were acquired with the Nicon Ax R microscope in the confocal mode with 100x/1.49 (oil immersion) objectives at a resolution of 1024 × 1024 pixels. The lasers used were

514 nm (for Ponceau 4R). The sample was loaded onto the slide and covered with a cover glass.

The preparation protocol for **C7SeO$_n$-H$_1$** adhesives: **C7SeO$_n$-H$_1$** is used to abbreviate samples with **C7SeO**: water (H) ratio of n: 1 (w/w). **C7SeO** and pure water were placed in a capped test-tube in defined ratios (w/w). The sample vial was heated at 80 °C for 1-4 hours until the sample's consistency matches the gel-like state described in the literature. [S4] The resulting **C7SeO**-water adhesive materials was then cooled to room temperature.

The preparation of the adhesive coating: the obtained crown-water adhesive materials were deposited on different substrates, then covered by another substrate. In order to homogenously cast the crown-water adhesive materials between two plates, a Farmar was placed onto the substrate-sample-substrate sandwich overnight.

The low temperatures adhesion tests: To obtain the lap shear strengths at low temperatures, the substrates adhered by **C7SeO$_{10}$-H$_1$** were stored in sealed bags and kept at low temperature for 24 hours, then it was tested quickly (tests can be finished within 20 s).

The adhesion tests of **C7SeO$_{10}$-H$_1$** in liquid nitrogen: The steel plates adhered by **C7SeO$_{10}$-H$_1$** were stored in liquid nitrogen for about 5 min. Then the lap-shear tests were finished quickly (within 20 s). In these tests, the temperature of the adhered steel plates was higher than -196 °C (about -185 °C ~ -180 °C).
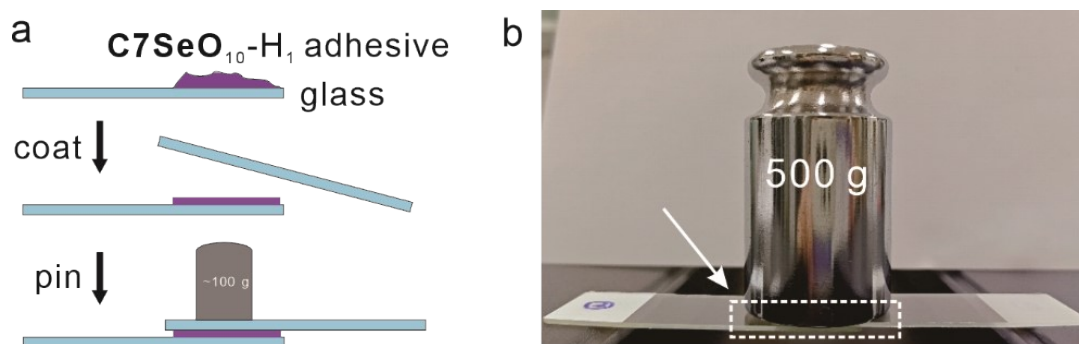
**Scheme S1.** The preparation of the adhesive coating.

Simulation Methods

The **C7SeO$_{10}$-H$_1$** sample in MD simulations contains 400 **C7SeO** molecules and 1000 water

molecules. Here, $C7SeO_{10}$-H_1 is used as an abbreviation for samples with a **C7SeO**: water (H) weight ratio of 10:1, the corresponding molar ratio is **C7SeO**:water = 1:2.5 (400:1000). The TIP4P/2005 potential are used to describe the water-water interaction. This model is an enhanced version of the TIP4P (Four-Site Transferable Intermolecular Potential) water model, and has been widely used in molecular simulations for more accurately describing water behaviour. [S5] **C7SeO** molecule are described by the general Amber force field (GAFF). [S6] Long range electrostatic interactions were treated by using the particle–particle particle–mesh method with a real-space cutoff distance of 12 Å. The 12-Åcutoff distance was also applied to the van der Waals interactions. The MD simulations are performed by using the GROMACS 2009 package in the constant-pressure and temperature (*NPT*) ensemble with a time step of 2.0 fs. [S7] The temperature was controlled by the Nosé–Hoover thermostat. The pressure is controlled by the Parrinello-Rahman coupling method at 1 bar. For a given temperature, the simulation time is 400 ns. Periodic boundary conditions are used in *xyz* directions. The spatial dimensions of the simulated box are $6.5 \times 6.5 \times 6.5$ nm^3 after equilibrium. Data of the last 20 ns are collected to analyse the structure of the system.

The geometries of **C7SeO**-H_2O complexes are optimized at using the density functional theory (DFT) at B3LYP/6-311++G(d,p) level [S8] with DFT-D3 correction. [S9] All DFT calculations are performed by using the Gaussian 09 software package. [S10] The strength of hydrogen bonds is estimated by the equation E_{HB} (kcal/mol) = -223.08*ρ_{BCP} (a.u.) + 0.7423, where ρ_{BCP} is the electron density at the bond critical point of hydrogen bonds. [S11] ρ_{BCP} is calculated by Multiwfn software. [S12]

2. Synthesis of compounds and analytical data

### 2.1 Preparation and characterization of selenoxide-containing crown ether C7SeO
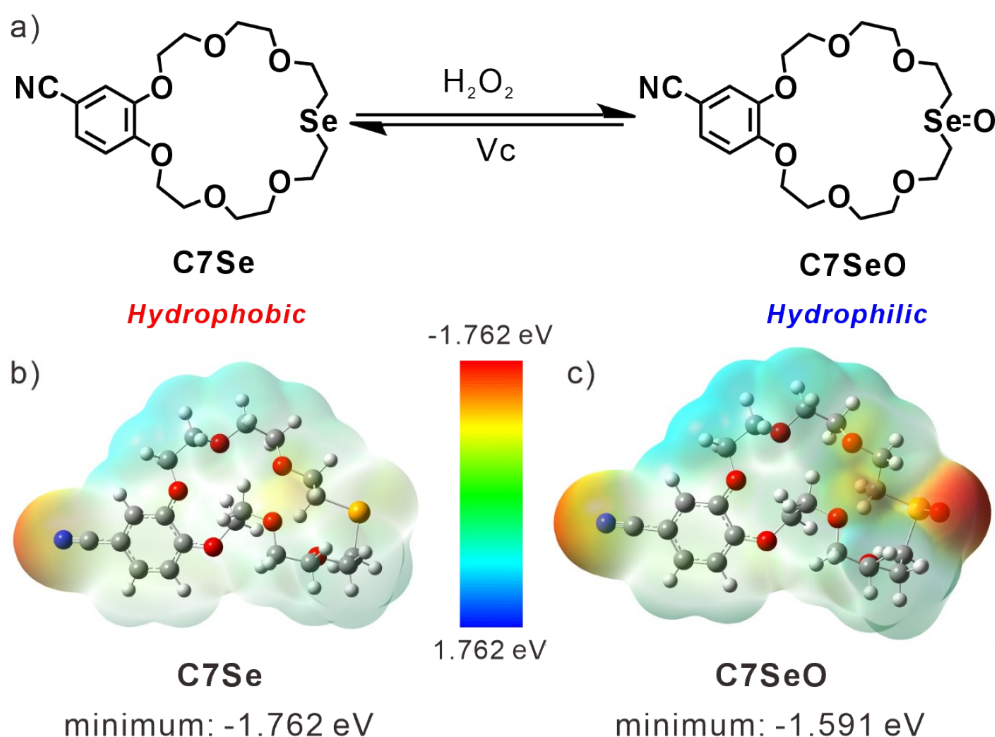
Figure S1. a) Synthetic route of **C7SeO**, b) and c) molecular electrostatic potential (MEP) maps of **C7Se** and **C7SeO**, obtained at B3LYP/6-311++G(d,p) level with DFT-D3 correction.

Compound **C7Se** (30 mg, 1.0 eq.) was dissolved in deionized water (6.75 mL) with a concentration below 10 mM. Subsequently, hydrogen peroxide (30%) (20.74 μL) was added to the solution. The mixture was stirred at room temperature (20 °C) for about 3 hours. The progress of the reaction was monitored by TLC until **C7Se** was completely consumed. Following this, the reaction mixture was filtered using a syringe filter (0.22 μm), and water was removed by freeze-drying for at least 48 hours. The resulting product was obtained as a white solid. ^{1}H NMR (500 MHz, CDCl$_3$, 298 K) δ = 7.28 (d, J = 1.9 Hz, 1H), 7.12 (d, J = 1.9 Hz, 1H), 6.90 (d, J = 8.4 Hz, 1H), 4.18 (dtd, J = 14.8, 5.0, 3.0 Hz, 4H), 4.05 – 3.84 (m, 8H), 3.77 – 3.64 (m, 8H), 3.41 (d, J = 13.2 Hz, 2H), 3.14 – 3.03 (m, 2H). ^{13}C NMR (126 MHz, CDCl$_3$, 298 K) δ = 152.94, 148.94, 127.03, 120.06, 119.17, 117.29, 113.71, 70.95, 70.88, 69.82, 69.65, 69.36, 68.96, 64.75, 64.65, 49.09; ^{77}Se NMR (95 MHz, CDCl$_3$, 298 K) δ = 852.97. HR-MS (ESI) m/z [M+Na]$^+$ *calcd.* for C$_{19}$H$_{27}$NNaO$_7$Se$^+$: 484.0845. *Found*: 484.0772.
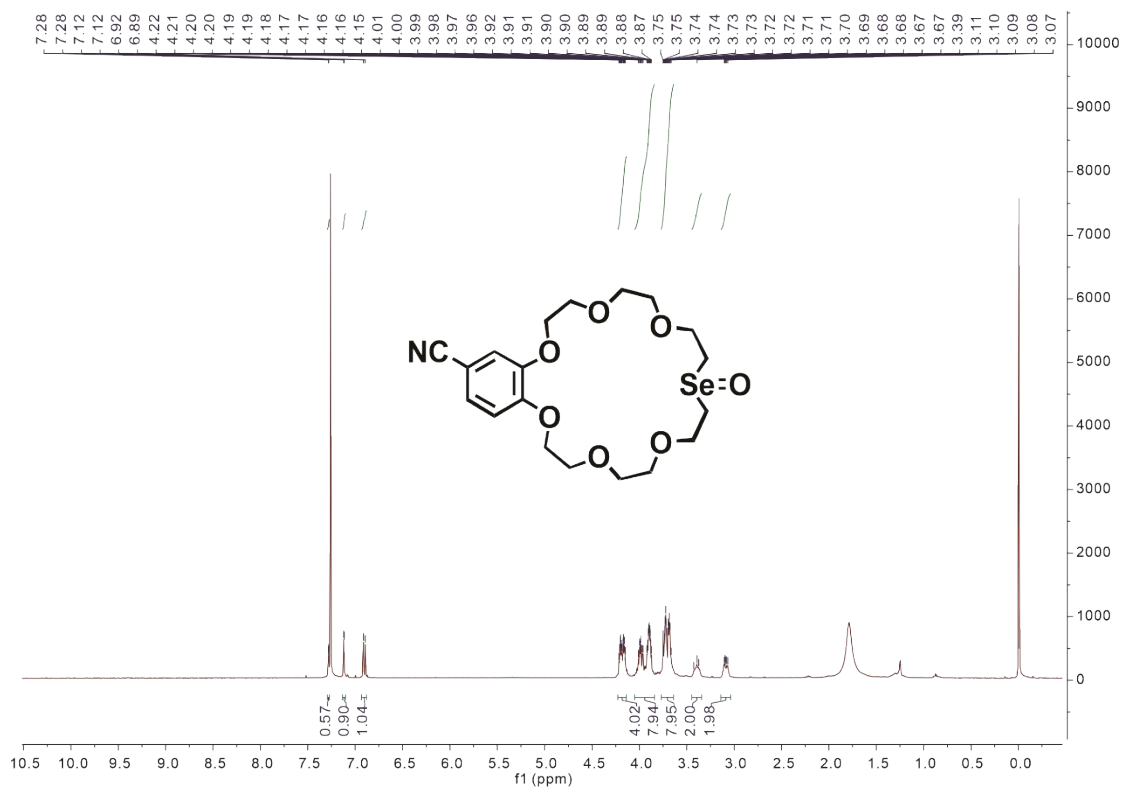
Figure S2. ^{1}H NMR spectrum (500 MHz, CDCl$_3$, 298 K) of **C7SeO**.
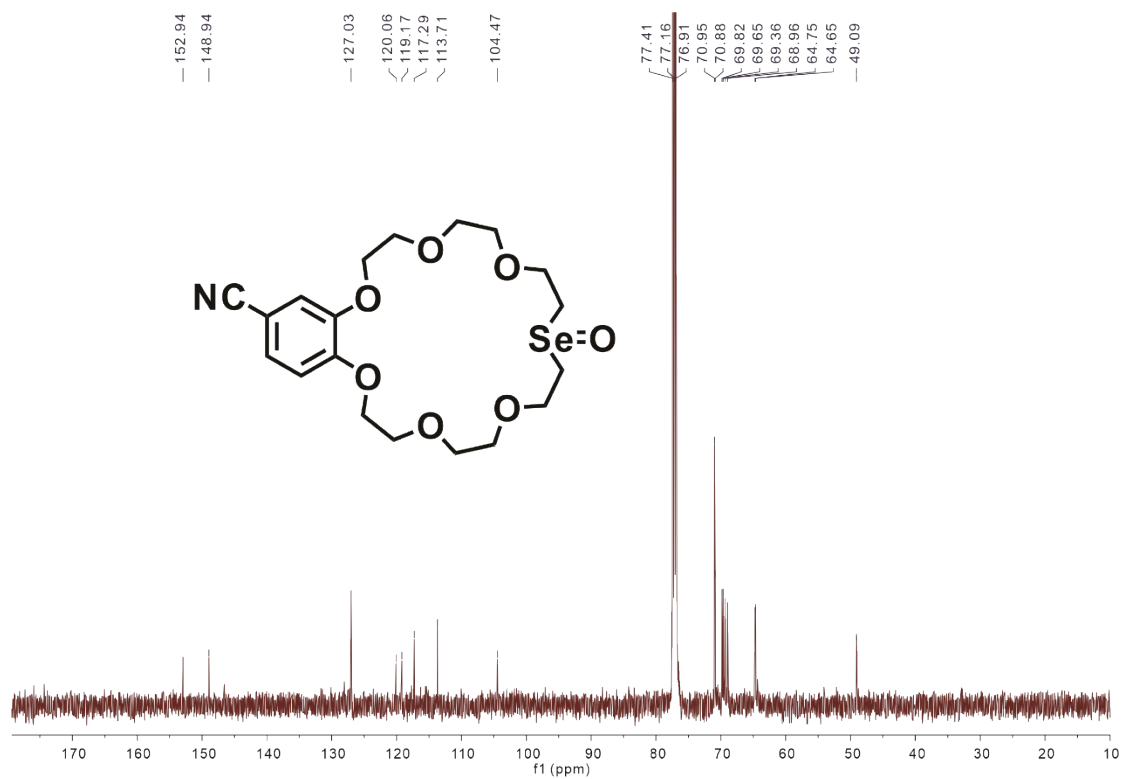
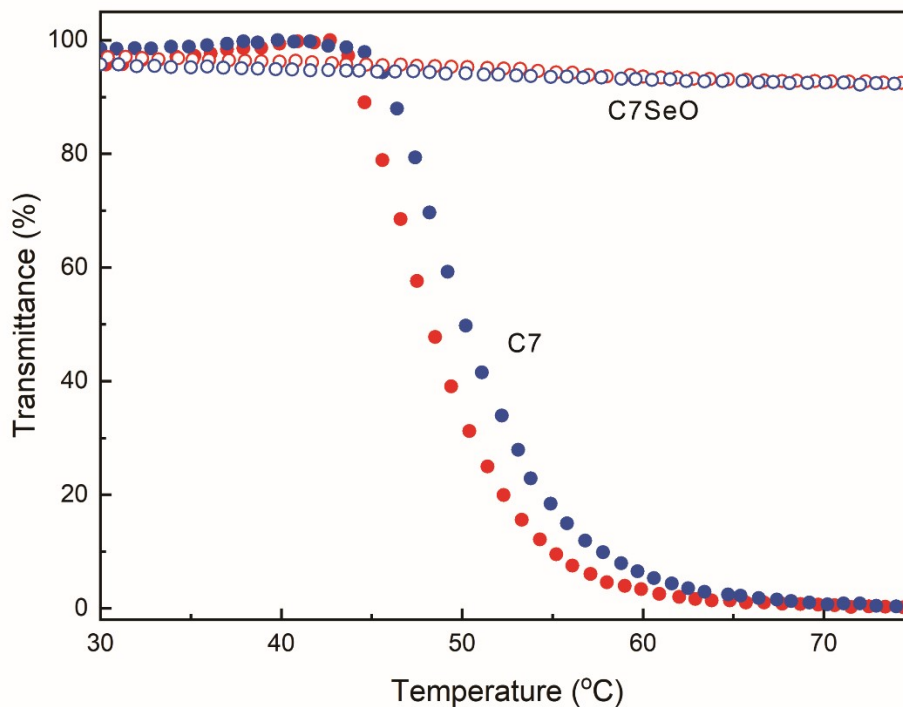***Figure S3.*** ^{13}C NMR spectrum (126 MHz, CDCl$_3$, 298K) of **C7SeO**.
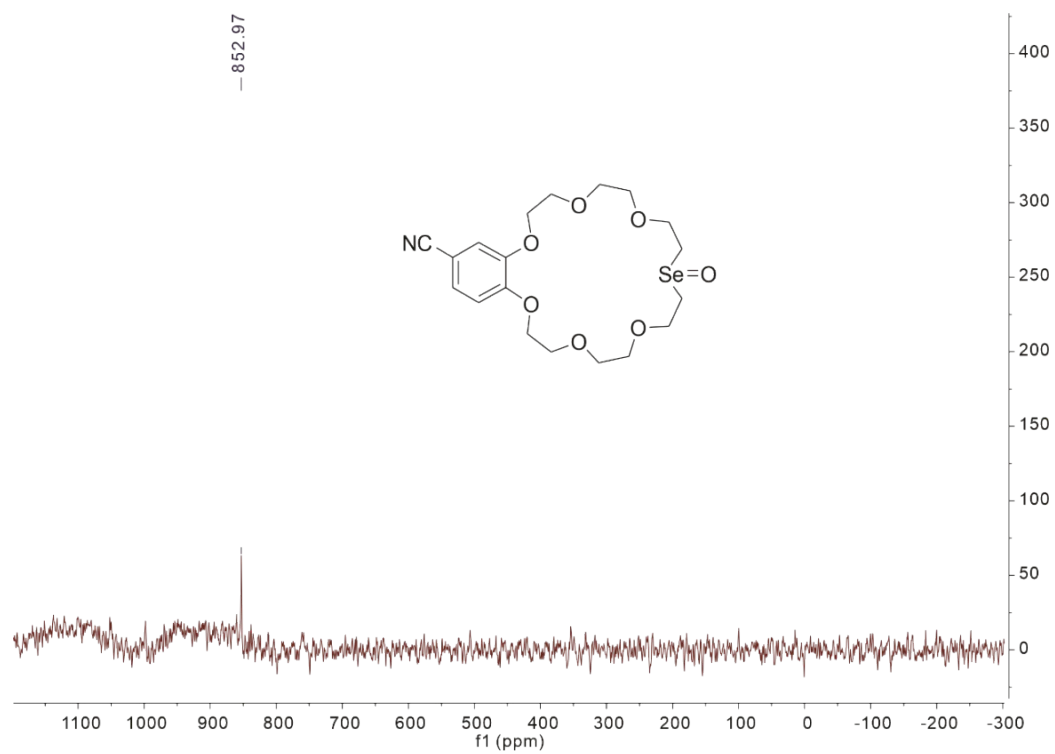
Figure S4. ^{77}Se NMR spectrum (95 MHz, CDCl$_3$, 298K) of **C7SeO**.
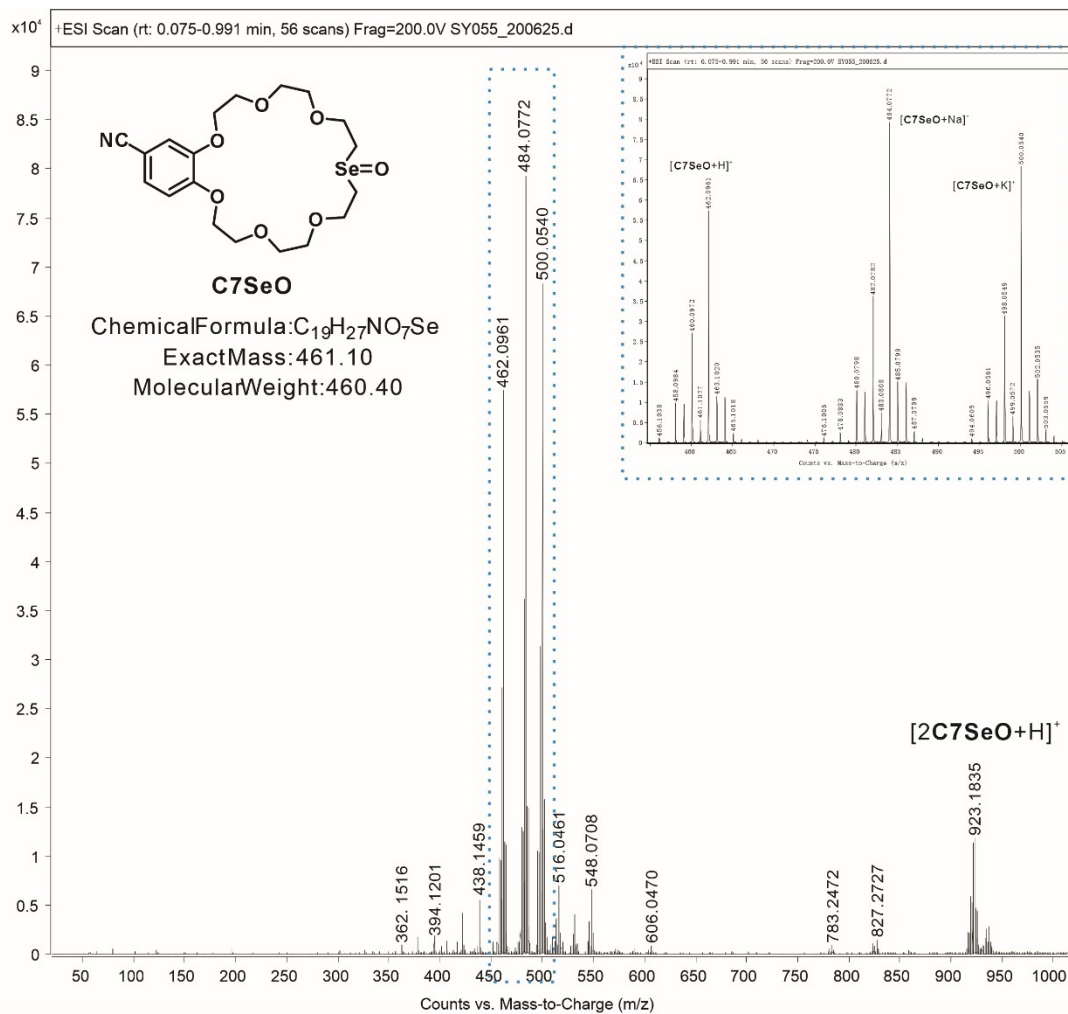
Figure S5. HR-MS of **C7SeO**.

## 2.2 Enhanced hydrogen bonding in C7SeO compared to C7

Figure S6. LCST of **C7SeO** and **C7** (100 mM) in water. The red dots represent the heating process, while the blue dots represent the cooling process.

The lower critical solution temperature (LCST) behavior can provide insights into hydration and hydrogen bonding. Compounds that show a lower critical solution temperature (LCST) behavior in an aqueous solution is soluble below LCST due to extensive hydrogen bonding interactions between crown ether and surrounding water molecules. When water molecules are repelled from the crown ring at elevated temperatures, hydrogen bonds between water and crown ether are broken resulting in a positive change in enthalpy. In addition, entropy increases as water molecules are no longer constrained. Hence, based on Gibbs free energy equation ($\Delta G = \Delta H - T\Delta S$), phase transition from clear (soluble) to turbid (insoluble) becomes spontaneous as the temperature gets above the threshold value (LCST) due to so-called "hydrophobic effect". The stronger hydrogen bond strength is, the higher LCST is. [S13] Compared to **C7**, there is only slightly decrease in transmittance at elevated temperature (even at 80 °C) in **C7SeO** aqueous solution, indicating stronger hydrogen bonding strength between **C7SeO** and water molecules.

2.3 DOSY NMR for C7SeO in aqueous solution states
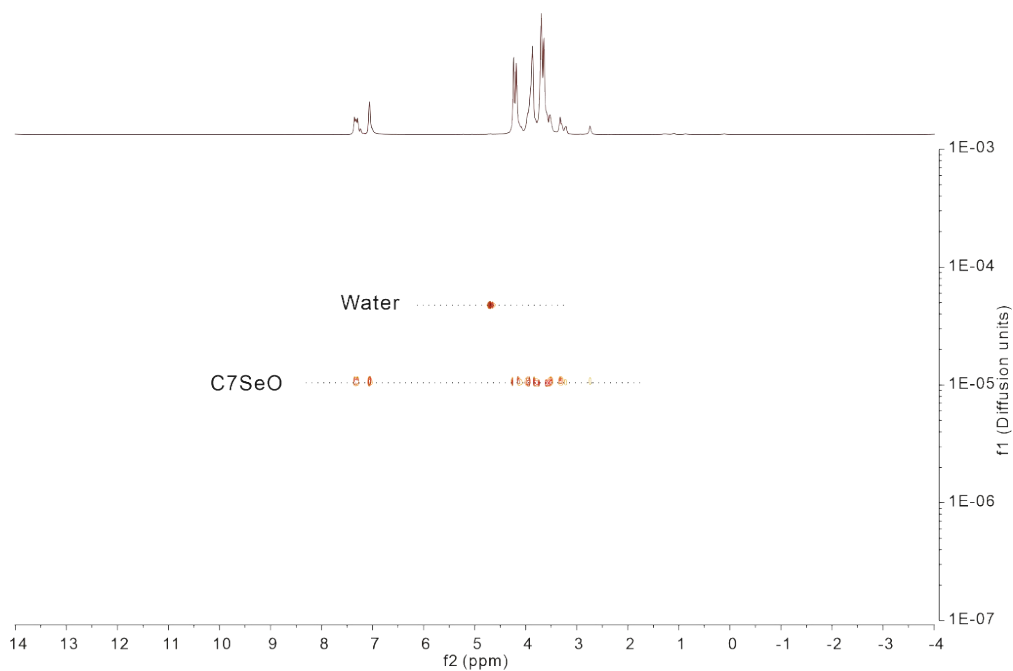
*Figure S7*. 2D DOSY spectrum (500 MHz, D$_2$O, 293 K) of **C7SeO** (10.0 mM).
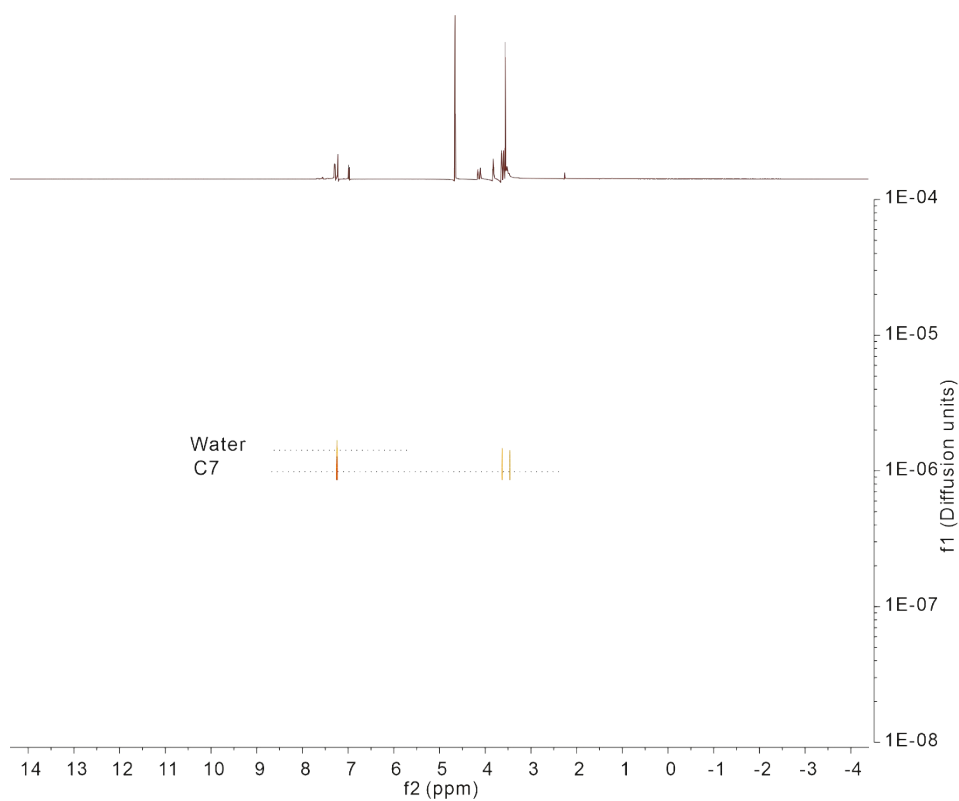
Figure S8. 2D DOSY spectrum (500 MHz, D$_2$O, 293 K) of **C7** (10.0 mM).

Compound	D (×10^{-10} m^2 s^{-1})	R_H (nm)	T2 (s)
C7SeO	1.07	2.29	0.44
C7	4.10	0.60	3.11

Table S1. DOSY NMR and T2 measurements of **C7SeO** and **C7** at 10 mM in D$_2$O at 25 °C. The hydrodynamic radii of the species were calculated according to the spherical approximation using the Stokes-Einstein equation: $D = k_B \cdot T/6\pi\eta R_H$, where k_B is the Boltzmann constant, T the absolute temperature, η the viscosity and R_H the hydrodynamic radius of the species under investigation. These results demonstrate that both of the two compounds not to from aggregates at 25 °C at 10 mM.

2.3 Concentration-dependent ¹H NMR of C7SeO
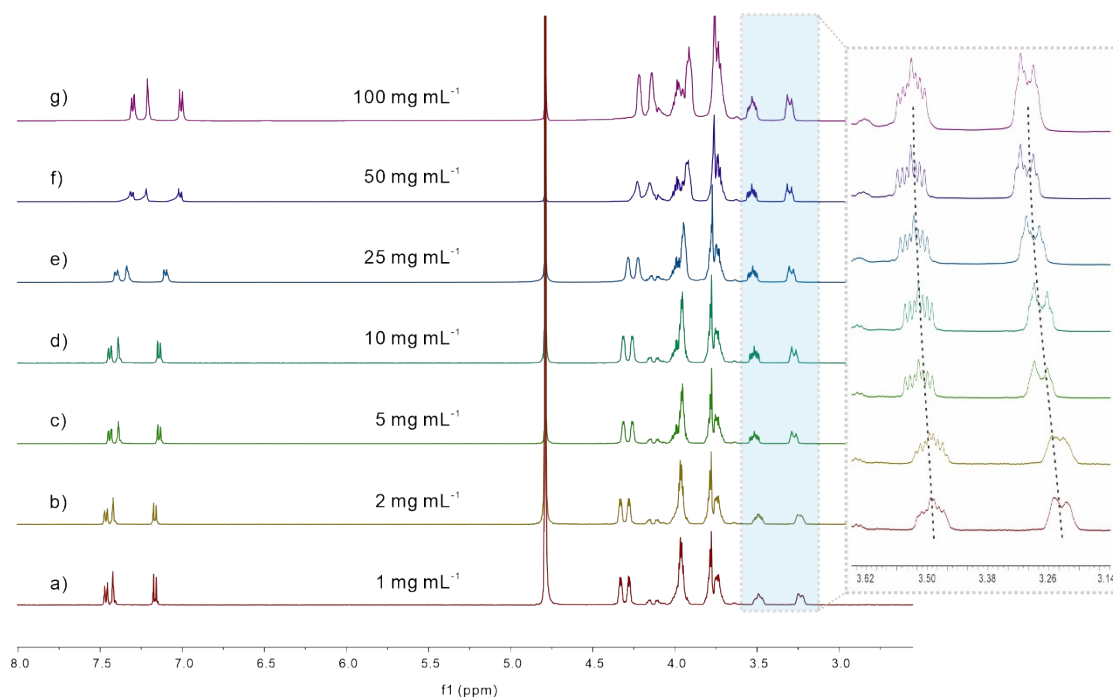
Figure S9. ¹H NMR spectra (500 MHz, D$_2$O, 298 K) of **C7SeO**. a) 1 mg mL^{-1}, b) 2 mg mL^{-1}, c) 5 mg mL^{-1}, d) 10 mg mL^{-1}, e) 25 mg mL^{-1}, f) 50 mg mL^{-1}, g) 100 mg mL^{-1}. Zoomed-in region of Figure S9, corresponding to the *CH$_2$* groups adjacent to the selenoxide.

In concentration-dependent ^{1}H NMR spectra in D$_2$O, noticeable peak shifts and broadening effects were observed at higher concentrations ($\geq$ 25 mg mL^{-1}), indicating the aggregation of **C7SeO** into polymeric structures.

2.4 Moisture absorption behavior of C7 and C7Se
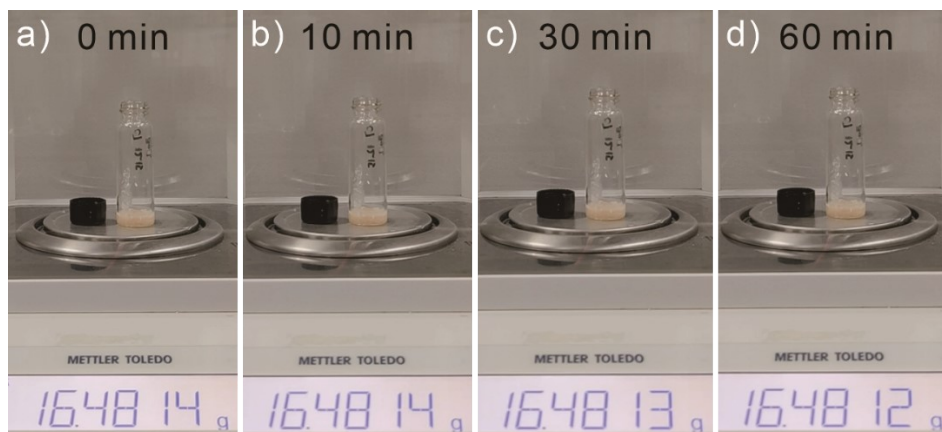
Figure S10. Moisture absorption behavior of **C7**.
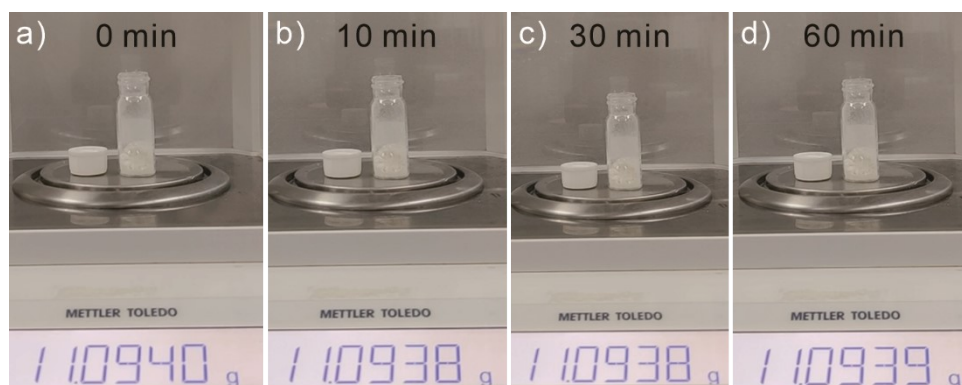
Figure S11. Moisture absorption behavior of **C7Se**.

From Figure S10 and S11, **C7** and **C7Se** did not show obvious moisture absorption behavior in ambient condition [25 °C, relative humidity (RH), 40%].

3. Confined water identification in supramolecular polymers

3.1 Dielectric Spectroscopy Evaluation of Complexed and Free Water Molecules

Broadband Dielectric Spectroscopy (BDS) offers a broad frequency range spanning in principle from 10^{-3} Hz to 10^{10} Hz. Within this extensive dynamic range, it is possible to investigate molecular fluctuations, charge transport mechanisms, and polarization effects at phase boundaries. This is

particularly true for investigating systems containing water due to the high dipole moment of water. Therefore, the behavior of water within supramolecular materials can be investigated by BDS. The molecular dynamics of water within the current supramolecular system are predominantly governed by its interactions with the materials themselves. Consequently, various states of water, such as bulk-like water, bonded water, and confined water, can thus be discerned and characterized. Furthermore, BDS will yield valuable insights into understanding the molecular mobility and the charge transport phenomena of water containing systems in both the dry and the wet state.
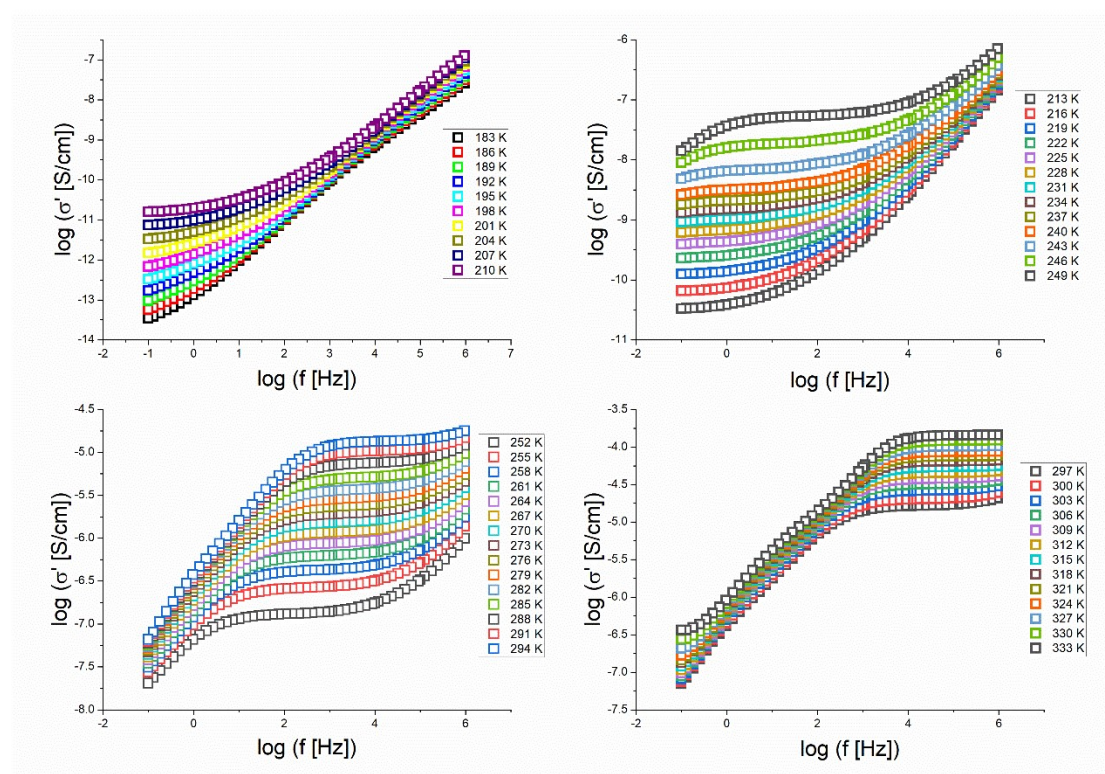

Figure S12. The real part of the complex conductivity *versus* frequency of a **C7SeO$_5$-H$_1$** adhesive at the indicated temperatures.

The frequency dependence of the real part of the complex conductivity spectra of **C7SeO$_5$-H$_1$** shows the typical conductivity-frequency behavior expected for semiconducting materials. [S14] The observed plateau in the data corresponds to the DC conductivity σ_{DC}. σ_{DC} is estimated by fitting the Jonscher equation to the data. [S15] The Jonscher equation reads
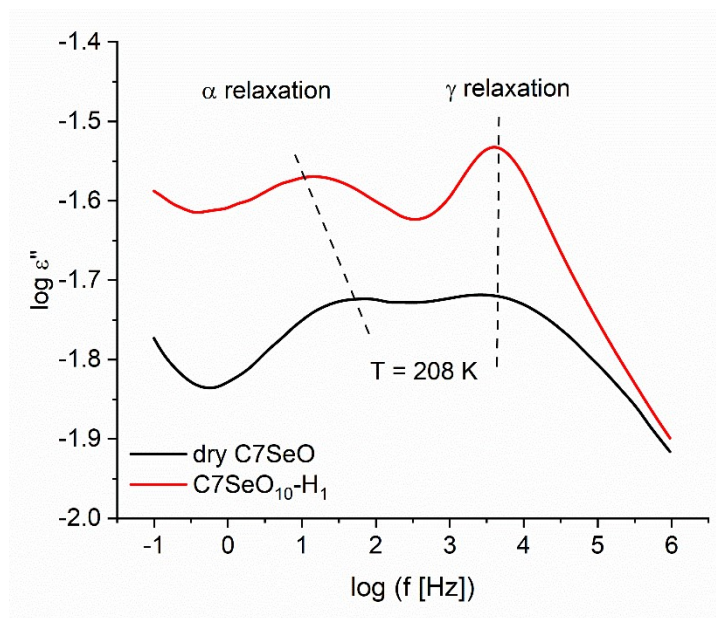
$$\sigma'(f) = \sigma_{DC}\left(1 + \left(\frac{f}{f_c}\right)^n\right)$$

The exponent n has values between 0.5 and 1. f_c is a characteristic frequency characterizing the onset of the dispersion.
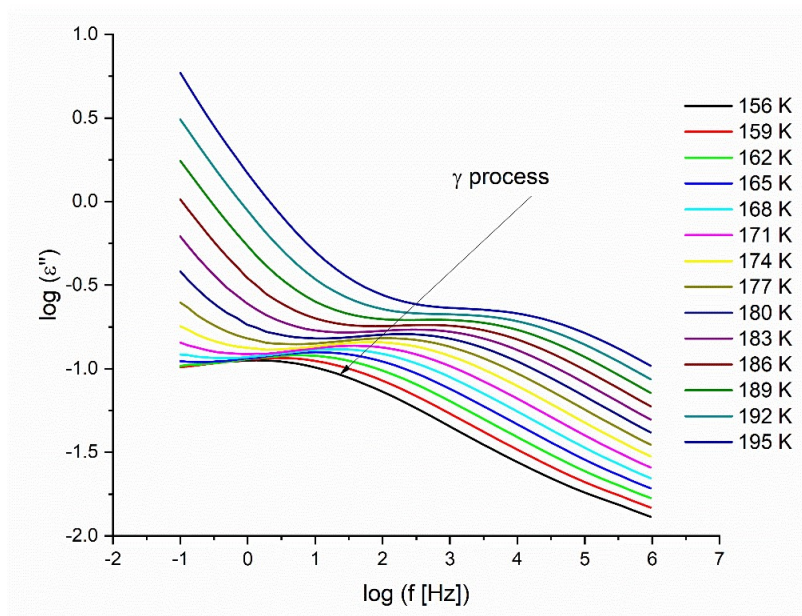

Figure S13. Dielectric loss *versus* frequency of a **C7SeO$_5$-H$_1$** adhesive at the indicated temperatures.

Figure S14. Dielectric loss *versus* frequency of **C7SeO$_{10}$-H$_1$** and dry **C7SeO** at 208 K.

For both samples γ processes and the α relaxation is observed. First, the absolute value of the

dielectric loss is higher for **C7SeO$_{10}$-H$_1$** compared to **C7SeO**. This is due to the higher dipole moment of the homogeneously incorporated water molecules. Secondly, for **C7SeO$_{10}$-H$_1$** the α relaxation shifts to lower frequency compared to the dry material. This shift points to an increased interaction due to hydrogen bonds between water and **C7SeO**.
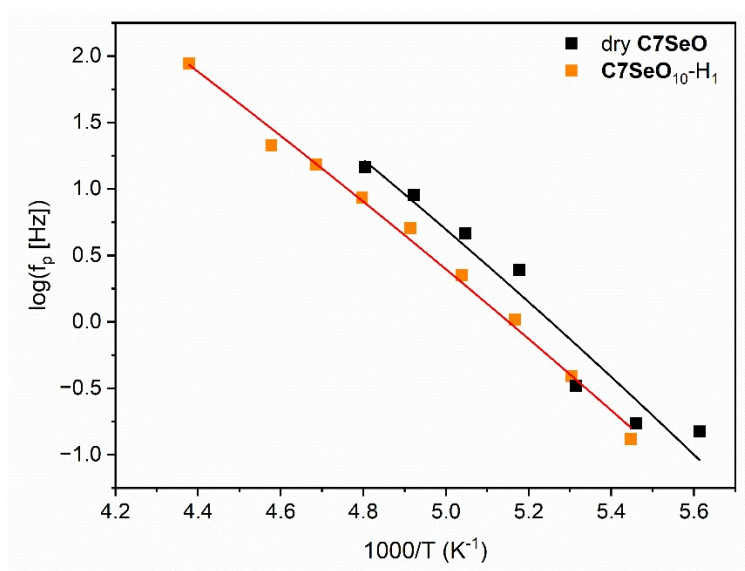
Figure S15. The frequency of α-relaxation *versus* temperature of **C7SeO$_{10}$-H$_1$** and dry **C7SeO**.

The α-relaxation is only clearly observed for the dry **C7SeO** and **C7SeO$_{10}$-H$_1$**. For **C7SeO$_5$-H$_1$** it is strongly overlaid by the conductivity contribution and the γ-relaxation. The data for **C7SeO** and **C7SeO$_{10}$-H$_1$** are close together which suggests that the α-relaxation is related to **C7SeO**.
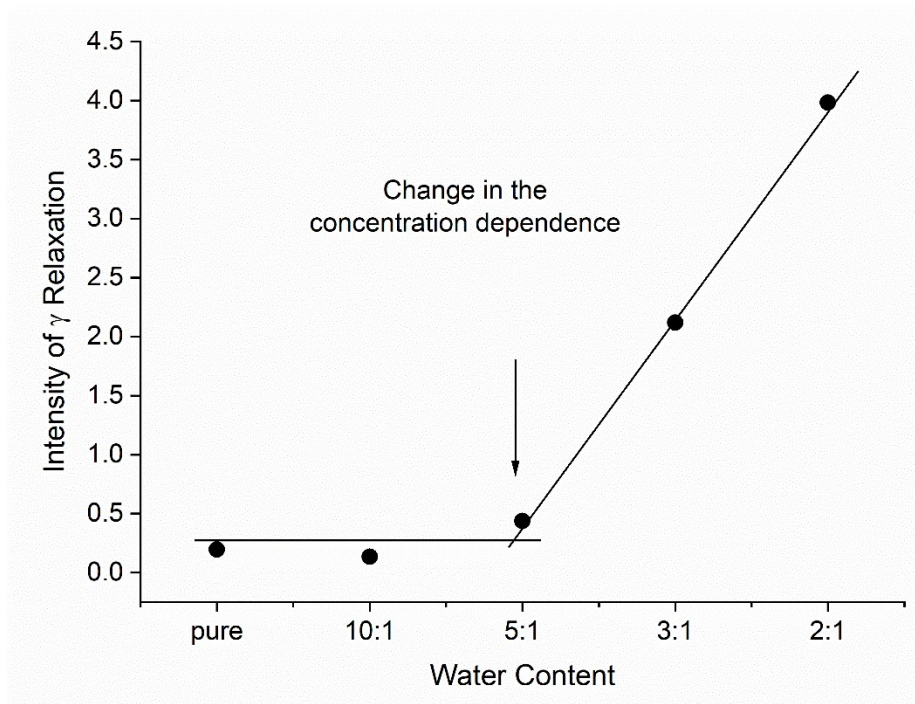
Figure S16. The intensity of γ-relaxation of **C7SeO$_n$-H$_1$** at 208 K.

From Figure S16, with the increase in the concentration of water, the intensity of the γ relaxation is approximately constant till the composition of 5:1. For higher concentration of water, the intensity of the γ relaxation increases strongly with the water content. Figure S16 displays two regimes in the concentration dependence indicating two different states of water in the system.

3.2 Flash-DSC measurement of $C7SeO_{10}$-H_1 materials

We apply fast scanning calorimetry (Flash-DSC), which can provide a heating rate more than four orders of magnitude higher than that of conventional DSC. This allows us to avoid the evaporation of water.
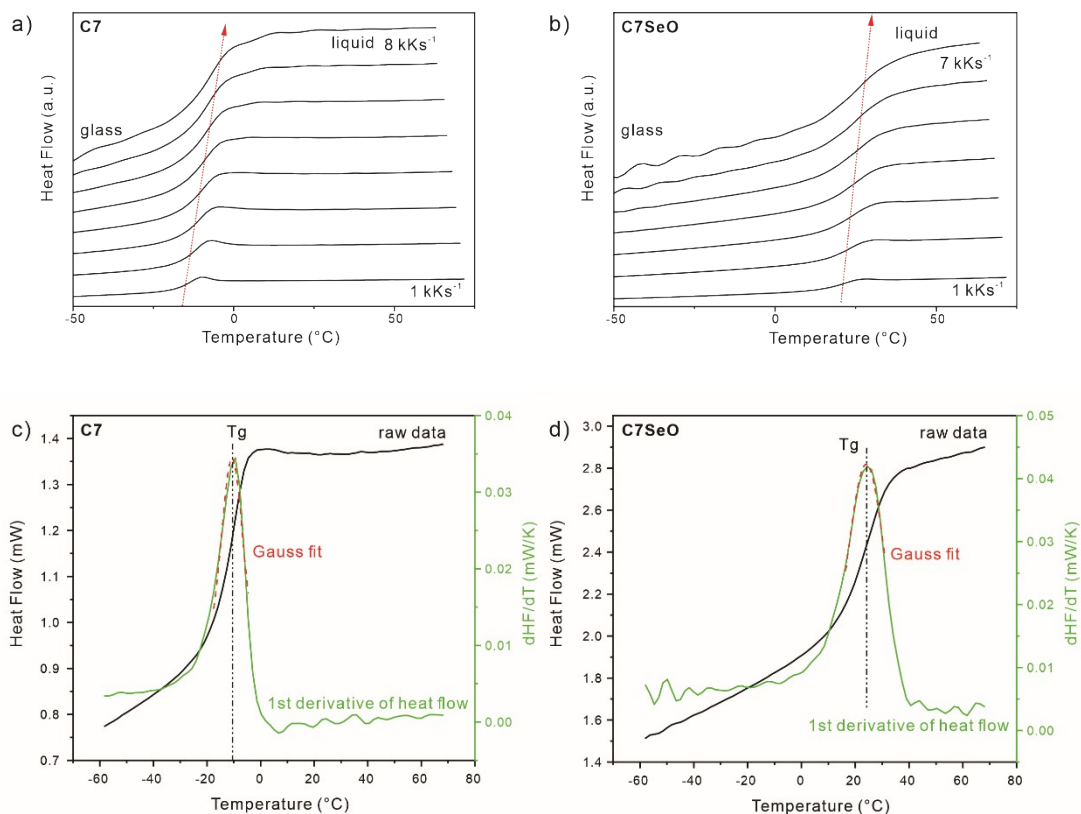
Figure S17. Flash DSC heat flow curves at heating rates ranging from 10^3 to $8*10^3$ K/s for a) **C7** and b) dry **C7SeO**. The glass transition is observed for c) **C7** and d) dry **C7SeO** at approximately 10 °C and 20 °C, respectively.

Heating Rate (K/s)	Tg(°C)				
	$C7SeO_2-H_1$	$C7SeO_3-H_1$	$C7SeO_5-H_1$	$C7SeO_{10}-H_1$	C7SeO
100	1.5	0.4	-17.1	-11.8	8.6
300	2.0	2.3	-12.7	-9.98	11.4
500	4.0	4.2	-10.1	-9.0	12.6
1000	6.4	6.2	-7.8	-6.9	16.8
2000	9.1	9.6	-4.3	-4.3	19,6
3000	11.6	10.9	-3.1	-2.72	20.7
4000	12.3	11.4	-	-	21.1
5000	13.8	12.6	-	-	
6000	14.0	-	-	-	
7000	14.9	-	-	-	

Table S2. Glass transition temperatures (T_g) of $C7SeO_n-H_1$ at different heating rates.
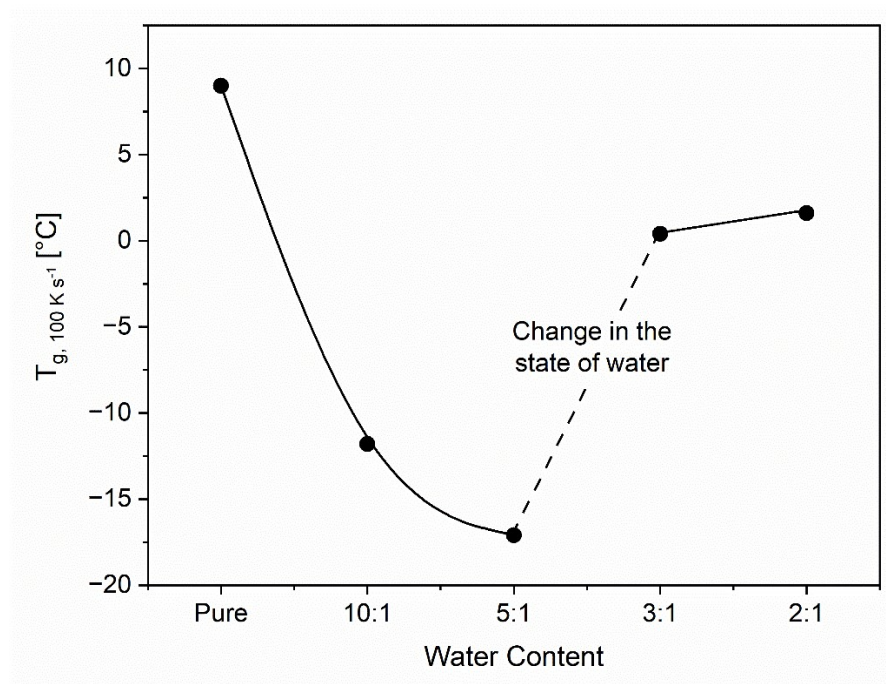
Figure S18. The glass transition temperatures (Tg) at 100 K/s for the **C7SeO$_n$-H$_1$** materials versus the water contents.

The Vogel-Fulcher-Tammann (VFT) formula is an empirical equation to describe thermos-kinetic data of glassy materials. [S17] For the heating rate β it is expressed as:

$$log\ \beta = \log \beta_\infty - \frac{A}{T - T_0}.$$

β_∞ is the heating rate reach infinite glass transition temperatures. T_0 is the so-called Vogel or ideal glass transition temperature. A is a fitting parameter which is related to an apparent temperature dependent activation energy.

3.3 TGA measurements of C7SeO$_n$-H$_1$ adhesive materials.
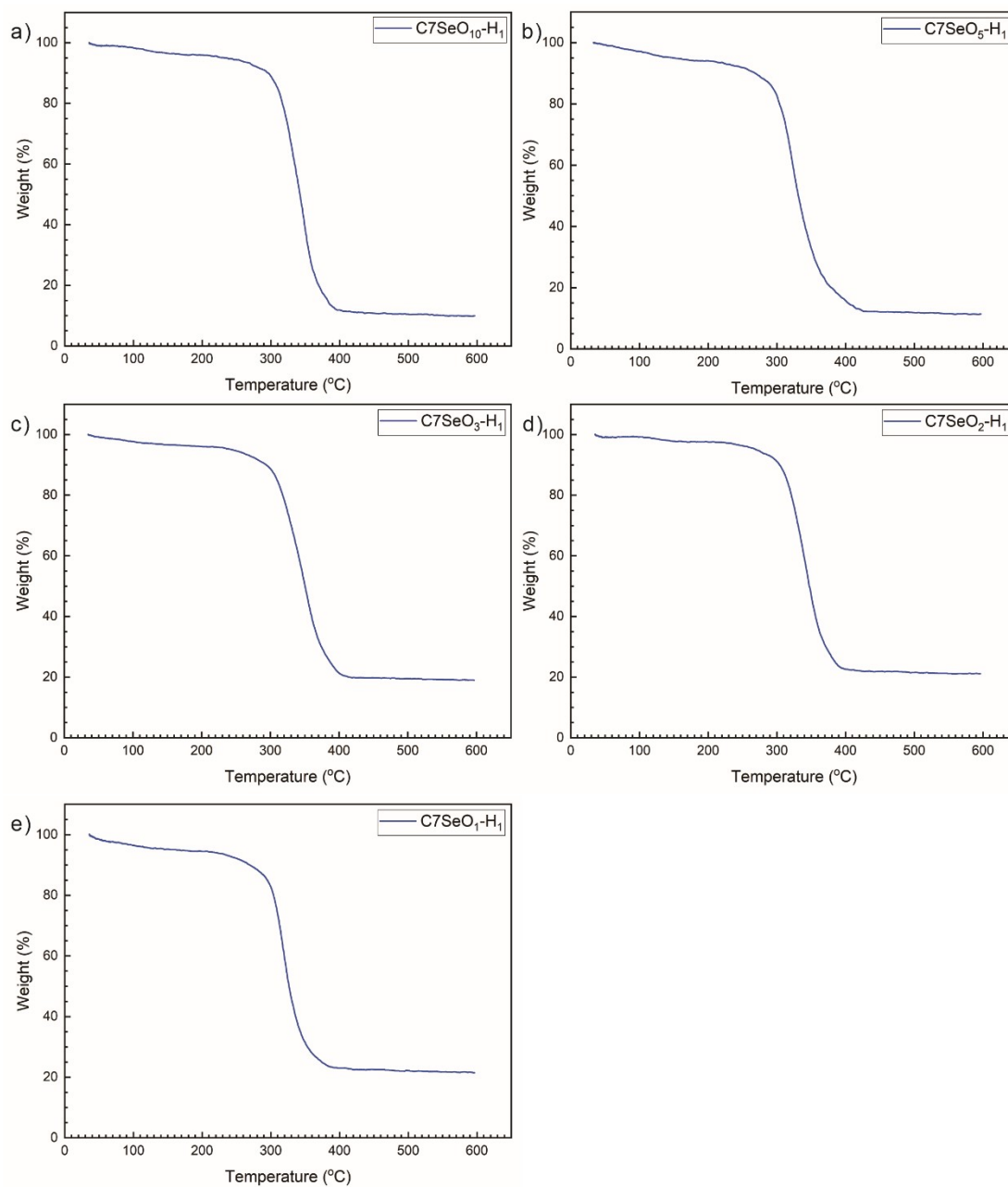

Figure S19. TGA measurements of **C7SeO$_n$-H$_1$** adhesive materials.

These TGA results demonstrate that **C7SeO** is stable at high temperature, and only starts to decompose above 300 ºC irrespective of the initial content of water.

Samples	Weight ratio of C7SeO to water	Molar ratio of C7SeO to water
$C7SeO_{10}:H_1$	10:1	1:2.5 (0.39)
$C7SeO_5:H_1$	5:1	1:5 (0.19)
$C7SeO_3:H_1$	3:1	1:8.5 (0.12)
$C7SeO_2:H_1$	2:1	1:12.8 (0.078)
$C7SeO_1:H_1$	1:1	1:25.6 (0.039)

Table S3. The weight ratio and molar ratio of $C7SeO_n$-H_1. The numbers in parentheses indicate the molar fraction of **C7SeO** to water.
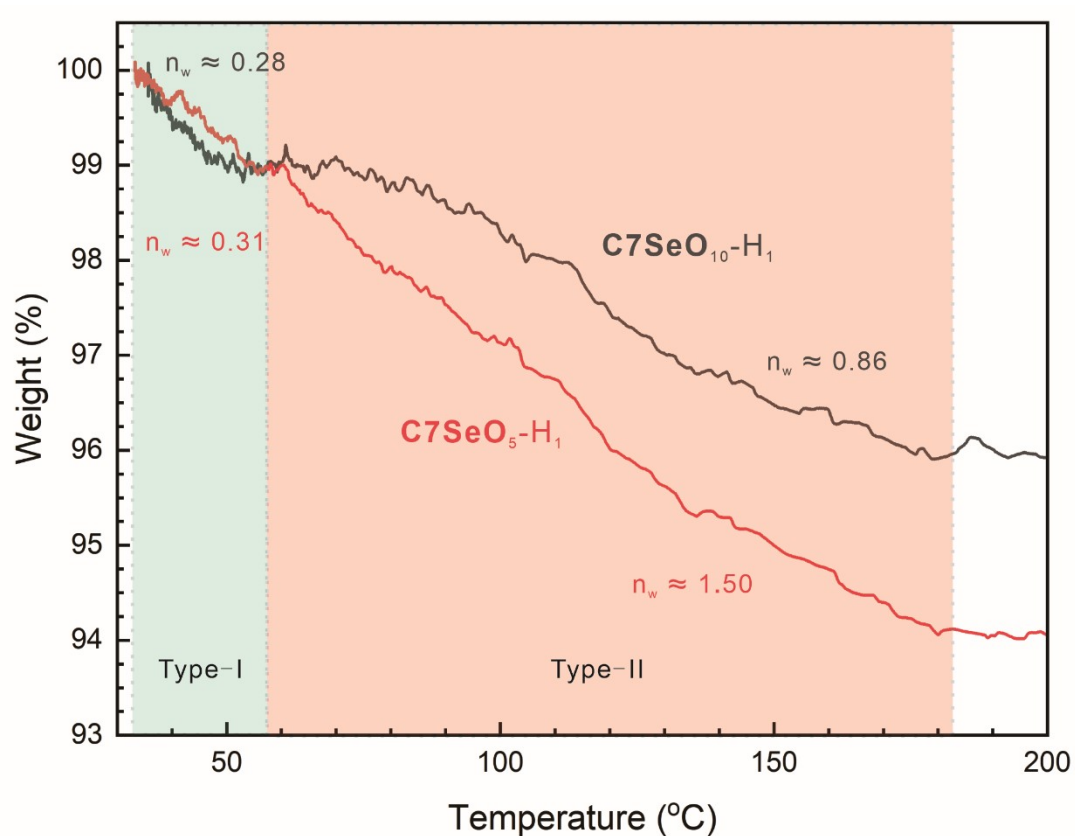
*Figure S20.* Segmented TG of $C7SeO_n$-H_1 (n = 10, 5) adhesive materials.

From the segmented TG of $C7SeO_n$-H_1 (n = 10, 5) adhesive materials, there are two stages in the desorption process of water. The water fraction that desorbs below 60 °C is labelled type-I, and

those requiring heating between 60–180 °C, type-II. Type-I water desorbs readily into dry nitrogen upon heating and is partially lost during the TG setup. Type-II water desorbs into nominally 'dry' nitrogen only at elevated temperatures. Type-II water has stronger bonding than Type-I water. [S18] In Figure S20, n_w is the mole ratio of desorbed water molecules in this stage to all the crown ether molecules in the sample, which indicates the degree of hydration. The calculation of Type-I water of **C7SeO$_{10}$-H$_1$** was used as an example:

$$n_w = \frac{\dfrac{m_{water}}{MW_{water}}}{\dfrac{m_{C7SeO(total)}}{MW_{C7SeO}}} = \frac{\dfrac{1}{100 \times 18.00}}{\dfrac{10}{(10 + 1) \times 460.3850}} = 0.28$$

Both the **C7SeO$_{10}$-H$_1$** and **C7SeO$_5$-H$_1$** samples show the very similar pattern as the temperature increases. As shown in Figure S20, two stages exist in both samples, type I n_w, type II n_w. The main difference is the amount of bound water, **C7SeO$_5$-H$_1$** showed higher type II n_w, which was roughly doubles compared to **C7SeO$_{10}$-H$_1$** under the same heating condition. This value is in accordance with the theoretical amount of water should have in **C7SeO$_5$-H$_1$** and **C7SeO$_{10}$-H$_1$**.
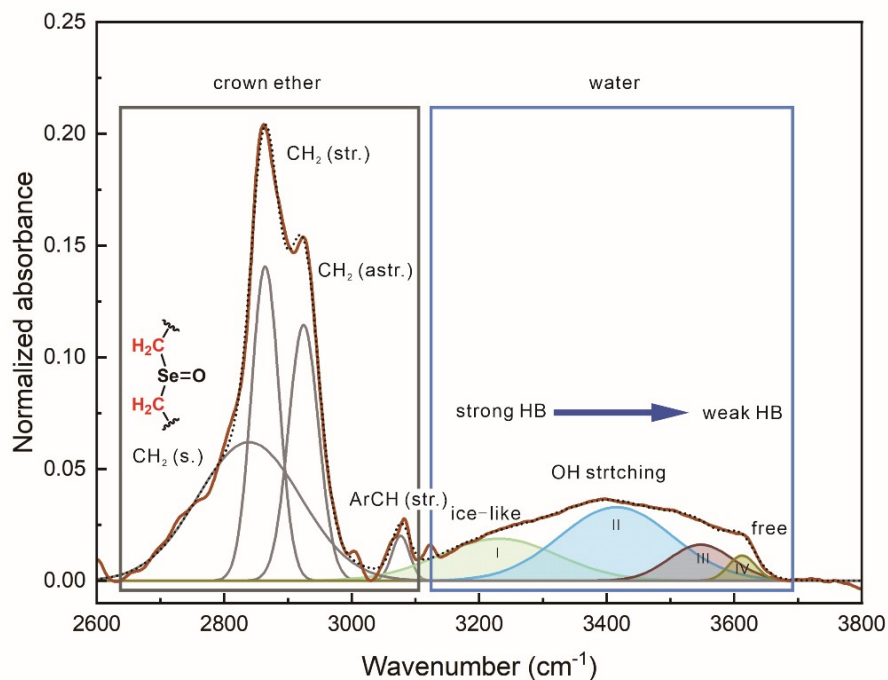
3.4 IR spectroscopy of C7SeO$_n$-H$_1$ materials
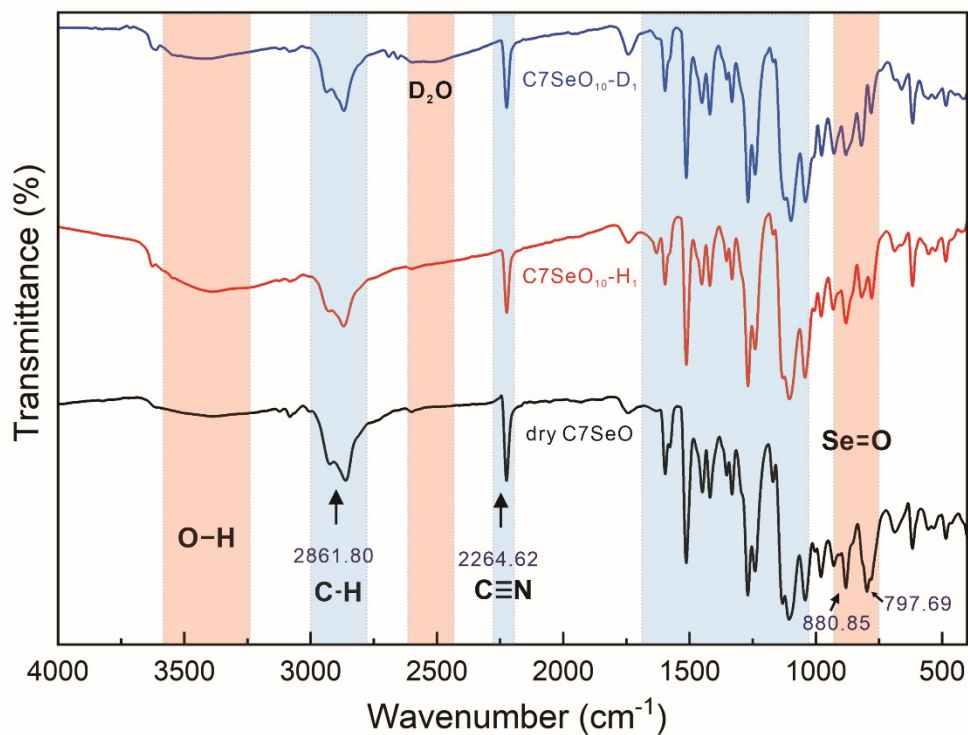
Figure S21. Full ATR-IR spectra of dry **C7SeO**, **C7SeO$_{10}$-H$_1$** and **C7SeO$_{10}$-D$_1$**.
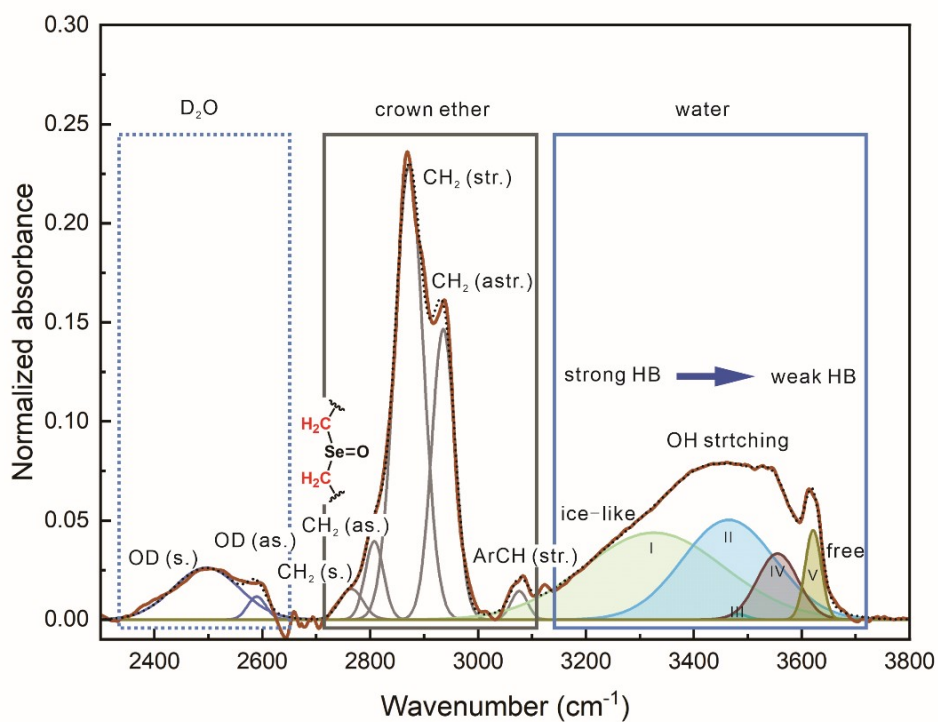
From Figure S21, compared to dry **C7SeO**, the selenoxide stretching peaks almost disappeared in the spectra of **C7SeO$_{10}$-H$_1$** due to the strong hydrogen bond between selenoxide and water molecules.

Figure S22. Fitting example of ATR-IR spectra in the region of 2600-3800 cm^{-1} of dry **C7SeO**. The OH stretching band was modelled with four Gaussian functions.

Figure S23. Fitting example of ATR-IR spectra in the region of 2300-3800 cm^{-1} of **C7SeO$_{10}$-D$_1$**. The OH stretching band was modelled with five Gaussian functions.
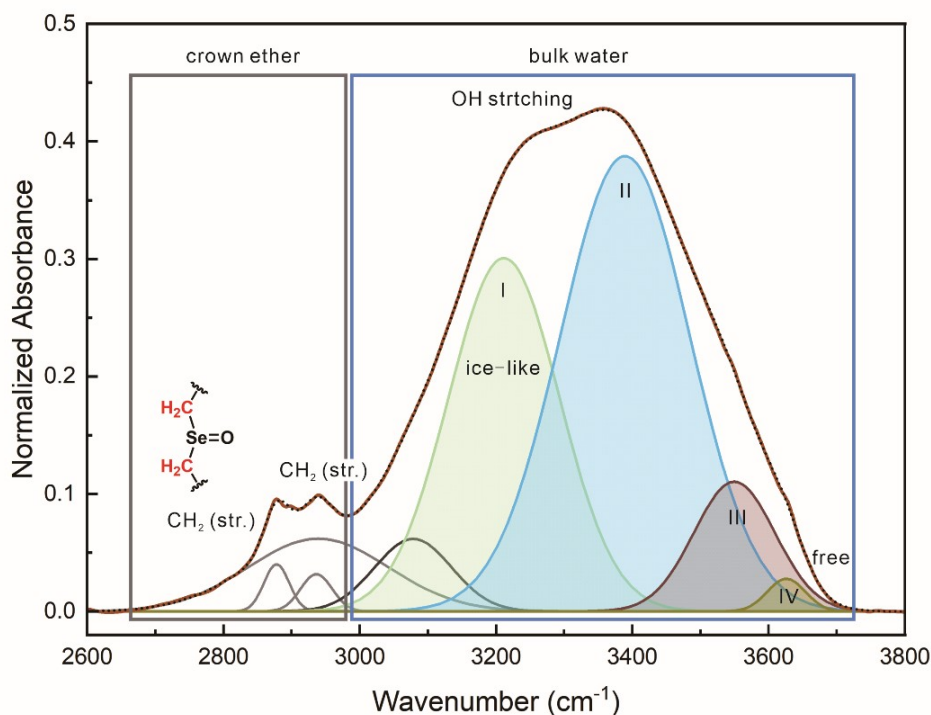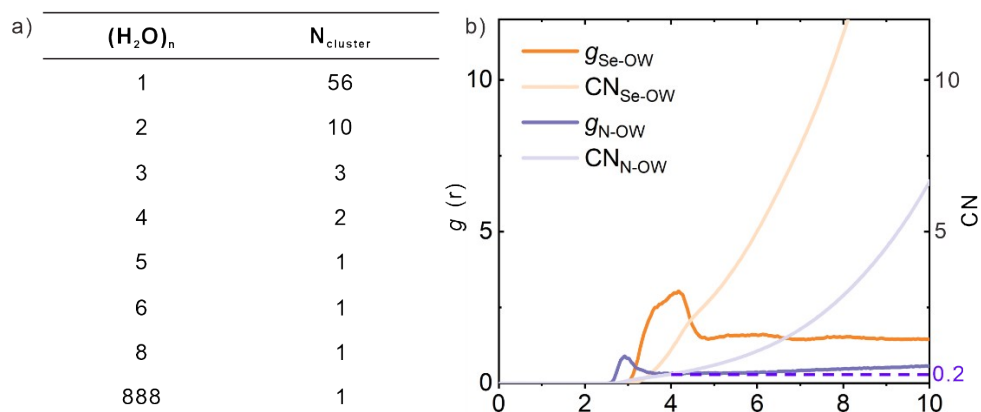
Figure S24. Fitting example of ATR-IR spectra in the region of 2600-3800 cm^{-1} of **C7SeO$_1$-H$_1$**. The OH stretching band was modelled with four Gaussian functions, which is similar to the assignments of five-Gaussian components of OH stretching in bulk water [S19].

3.5 All-atom molecular dynamics (MD) simulations of C7SeO$_n$-H$_1$ materials

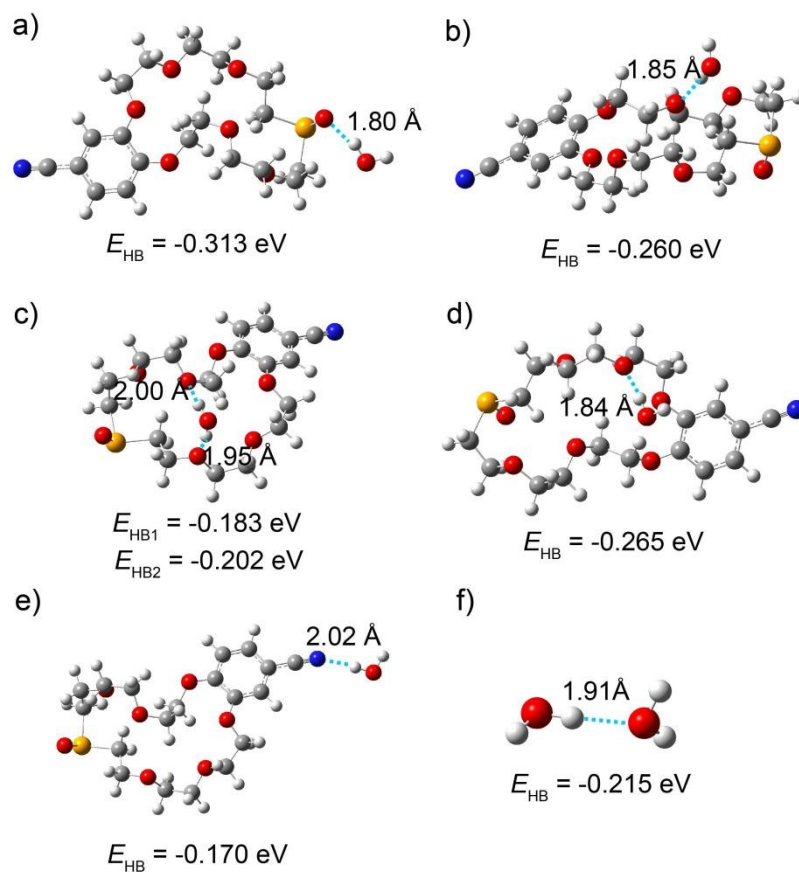| (H$_2$O)$_n$	N$_{cluster}$
1	56
2	10
3	3
4	2
5	1
6	1
8	1
888	1

Figure S25. a) The system in Figure 4a contained a large water ball (~888 water molecules), 56 water monomers, 10 water dimers, 3 water trimers, 2 water tetramer, 1 water pentamer, 1 water hexamer, 1 water heptamer and 1 water octamer. b) g_{Se-OW} and g_{N-OW}, and corresponding CN$_{Se-OW}$ and CN$_{N-OW}$, respectively.

| $(H_2O)_n$	$N_{cluster}$
1	61
2	12
3	7
4	4
5	1
6	1
7	2
836	1
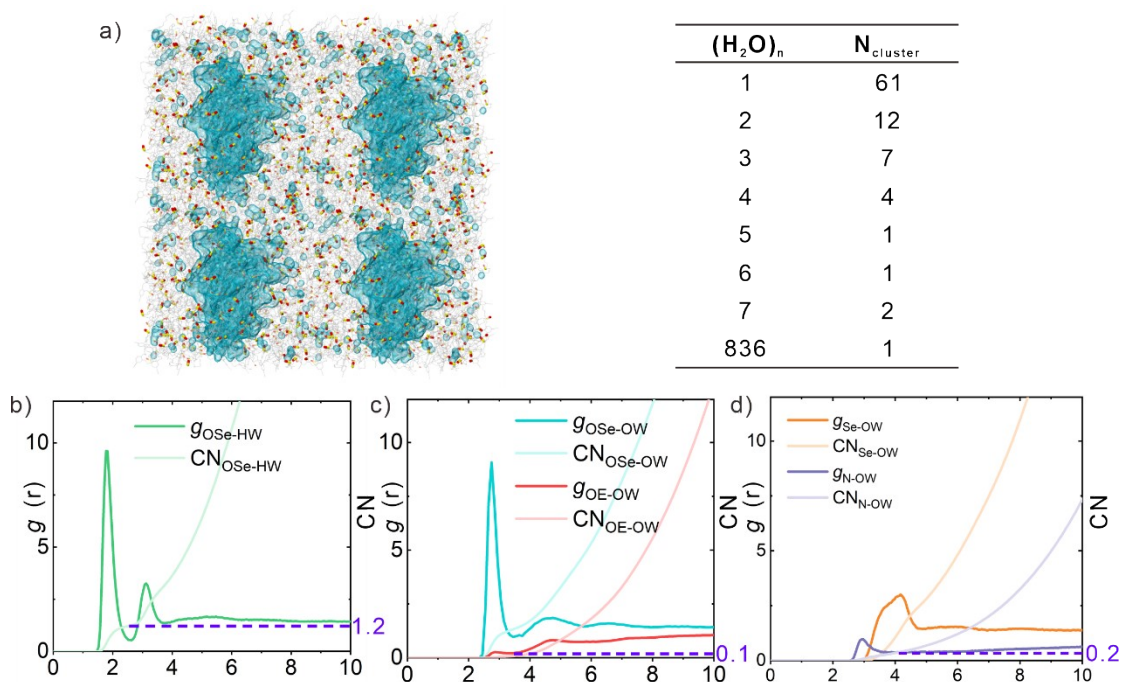
Figure S26. a) Snapshot from (MD) simulations of the **C7SeO$_{10}$-H$_1$** materials at 270 K. b) g_{OSe-HW} and corresponding CN$_{OSe-HW}$. c) g_{OSe-OW} and g_{OE-OW}, and corresponding CN$_{OSe-OW}$ and CN$_{OE-OW}$. (d) g_{Se-OW} and g_{N-OW}, and corresponding CN$_{Se-OW}$ and CN$_{N-OW}$, respectively.

Similar to the **C7SeO$_{10}$-H$_1$** system at 240 K, when the temperature increased to 270 K, the system contained a large water ball (~836 water molecules), 61 water monomers, 12 water dimers, 7 water trimers, 4 water tetramer, 1 water pentamer, 1 water hexamer, and 2 water heptamer (Figure S26a). The SeO-water hydrogen bond was ~1.80 Å, and each selenoxide group could form ~1.2 hydrogen bonds with water molecules (Figure S26b). The nearest distance between O atom in selenoxide group and O atom in water molecules was also 2.76 Å (Figure S26c). However, the number of water molecules around ether groups and cyano groups was only 0.1 and 0.2, respectively, which suggested that there were nearly no water molecules around ether groups and cyano groups (Figure S26 c and d).

a) E_{HB} = -0.313 eV

b) E_{HB} = -0.260 eV

1.80 Å

1.85 Å

c) 2.00 Å 1.95 Å
E_{HB1} = -0.183 eV
E_{HB2} = -0.202 eV

d) 1.84 Å
E_{HB} = -0.265 eV

e) 2.02 Å
E_{HB} = -0.170 eV

f) 1.91Å
E_{HB} = -0.215 eV

Figure S27. Optimized structure and estimated hydrogen bond strength of **C7SeO**-H_2O complex with O atom of a) selenoxide group, b-d) ether group and e) cyano group acting as the hydrogen bond acceptor. f) water dimer. All structures are optimized at B3LYP/6-311++G(d,p) level with DFT-D3 correction.

# 4. Low temperature adhesives of C7SeO$_n$-H$_1$ materials
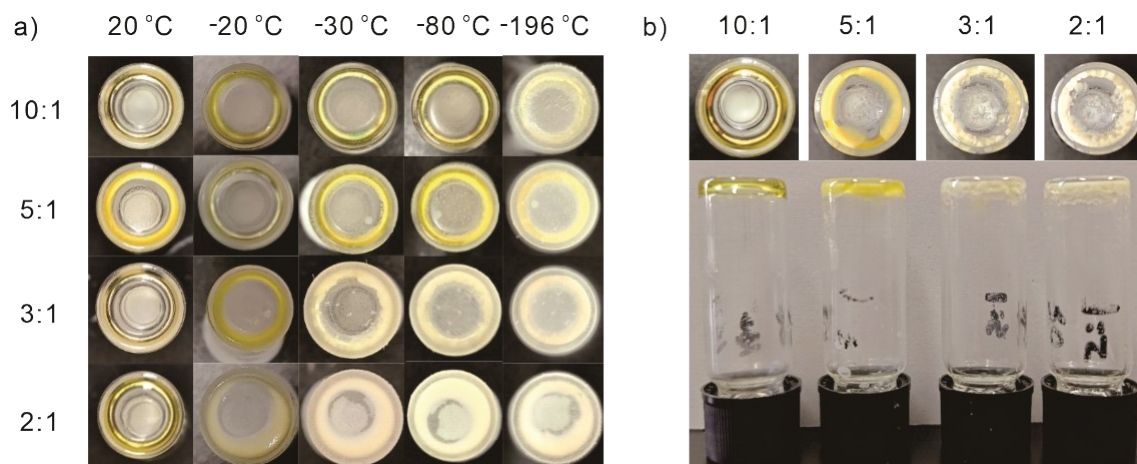
Figure S28. Macroscopic view of **C7SeO$_n$-H$_1$** (n = 10, 5, 3, 2) a) at different sub-zero and extremely low temperatures; b) rewarmed to room temperature.

As shown in Figure S28a, **C7SeO$_{10}$−H$_1$** is tolerant to low temperatures. There are no cracks in the sample until the temperature decrease to -20 °C, only fewer cracks were observed in the low temperature range (from -30 to -80 °C), indicating that **C7SeO$_{10}$−H$_1$** is flexible enough at low temperatures. Bulk cracks appeared when cooled in liquid nitrogen, which also significantly depressed the adhesion performance of **C7SeO$_{10}$−H$_1$** after immersed in liquid nitrogen (Figure 5c). Meanwhile, it is obvious that the low-temperature resistance of the **C7SeO−**water copolymer is closely related to its water content. High-water-content **C7SeO$_n$−H$_1$** samples became turbid solids at low temperatures. Carefully analyzing the turbid solids demonstrated that the water in these samples turned to ice. [S20] These differences are ascribed to the different functions of water molecules: in high-water-content **C7SeO$_n$−H$_1$** samples, water is used to solvate **C7SeO** molecules; hence, there are no polymeric supramolecular structures, and these samples behave more like bulk water than viscous supramolecular polymers. However, in **C7SeO$_{10}$−H$_1$** sample, water molecules play a role of "confined water", which are tightly bonded to **C7SeO** molecules. These results are consistent with BDS measurements.

When **C7SeO$_n$−H$_1$** samples were warmed to room temperature, **C7SeO$_{10}$−H$_1$** returned to its original state completely, indicating that the **C7SeO** molecules remain firmly bonding with water molecules as inseparable units in the polymeric structure during the cooling-warming process, preventing the

aggregation/crystallization of water and the structural destruction of the polymeric structure. However, the other samples (n = 5, 3, 2) showed varying degrees of structural destruction.
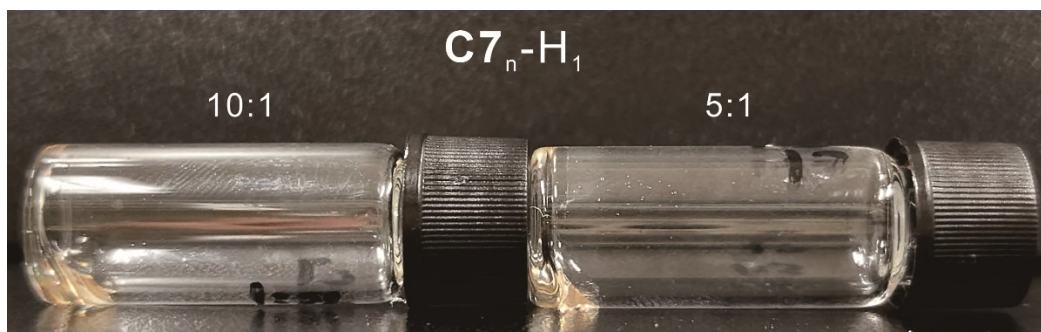
**Figure S29.** Macroscopic view of $C7_n$-H_1 (n = 10, 5) at room temperature.

As shown in Figure S29, $C7_n$-H_1 samples are transparent and viscous glue-like material with low viscosity.
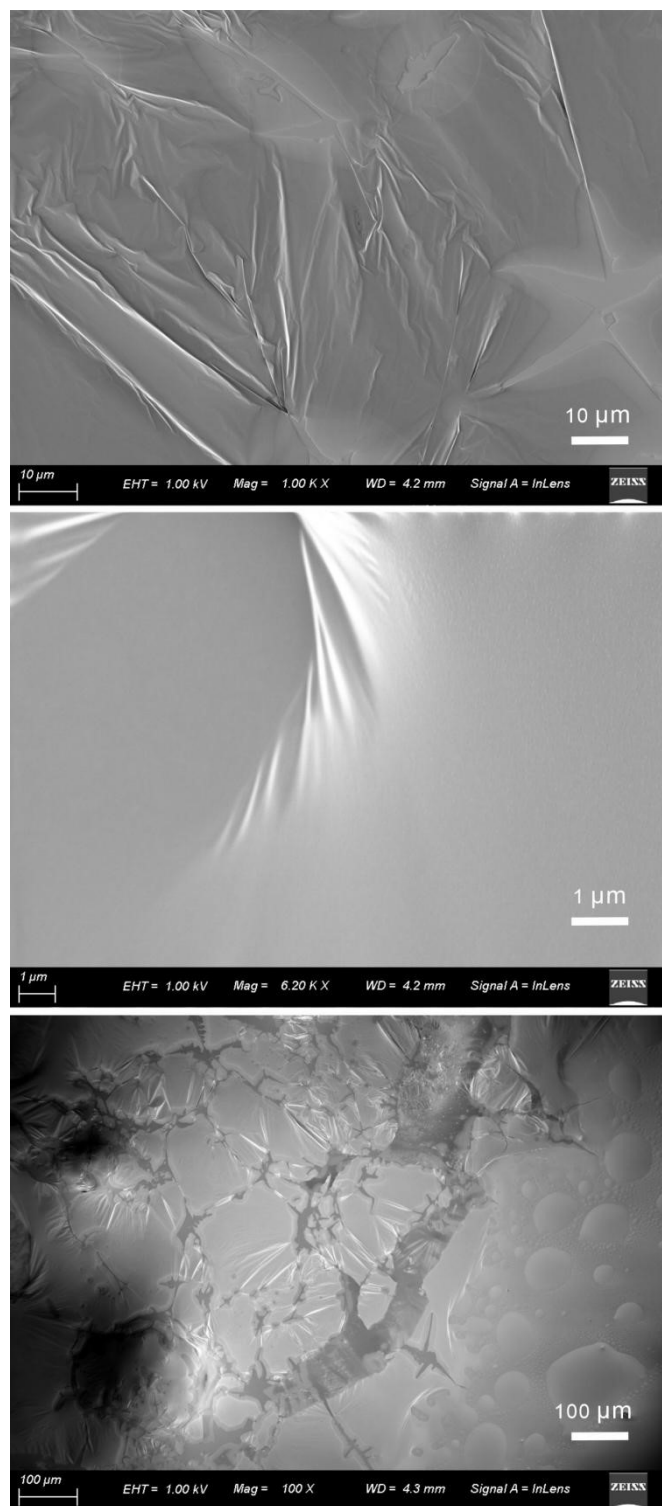
Figure S30. SEM images of **C7SeO$_{10}$**-H$_1$ at 25 ^{o}C.

No detailed structures, such as fibers and three-dimensional networks, were found in the **C7SeO$_{10}$**-H$_1$ sample, indicating that the morphology properties of confined water polymeric adhesives and supramolecular polymer gels are different.
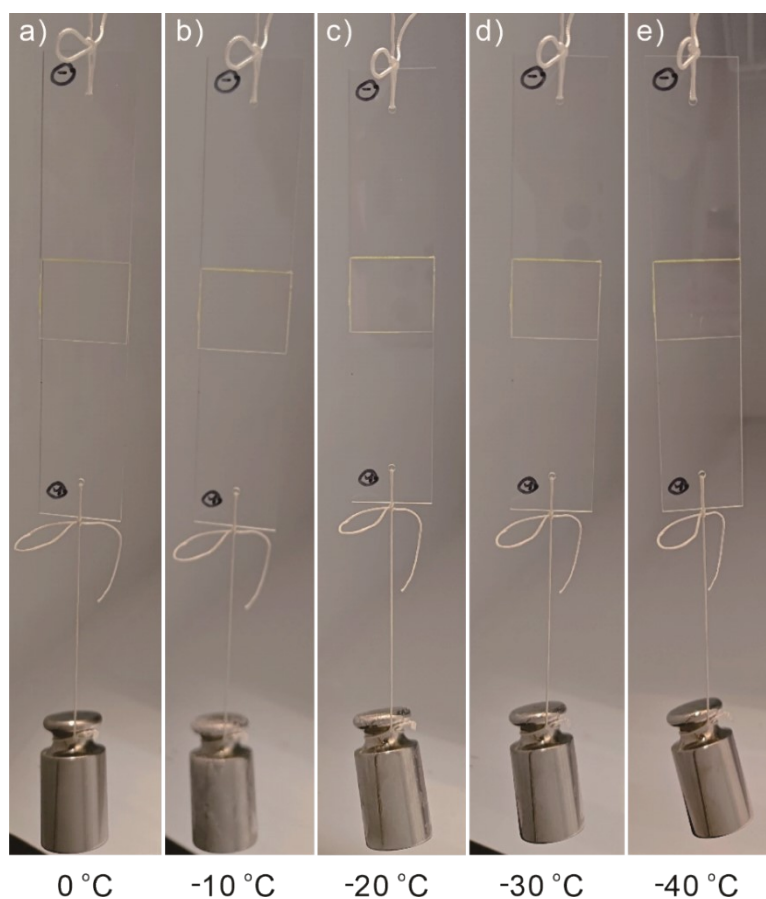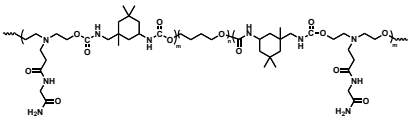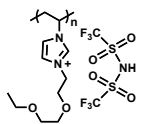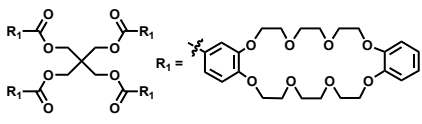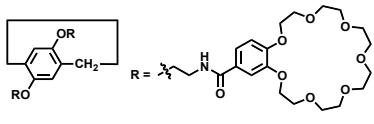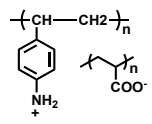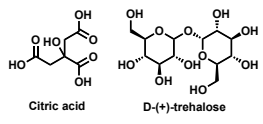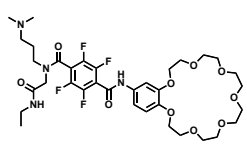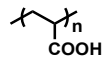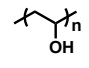
Figure S31. Macroscopic adhesive tests of **C7SeO$_{10}$-H$_1$** on glass (25 mm × 20 mm) at different temperatures. The weight of the Farmar is 100 g.
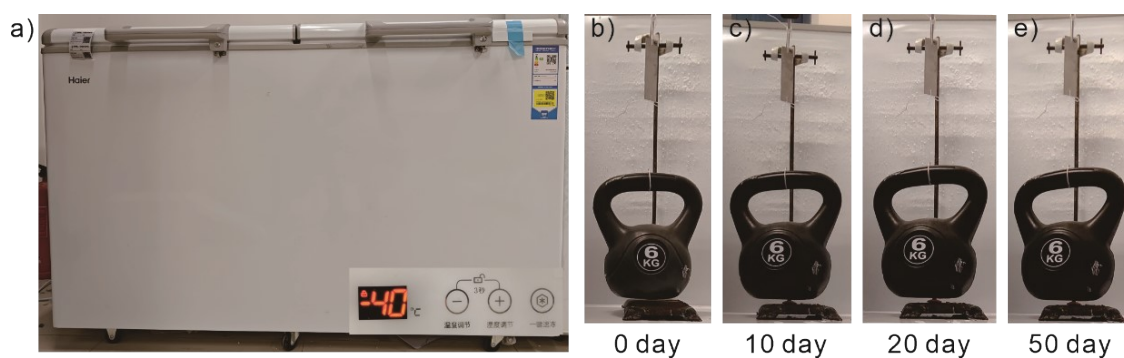
Figure S32. Time-dependent adhesion performance of **C7SeO$_{10}$-H$_1$** on steel at -40 °C. In this experiment, a refrigerator was used to maintain a constant low temperature, and a 6 kg dumbbell was utilized.

The **C7SeO$_{10}$-H$_1$** adhesion exhibit good low-temperature resistant and long-term stability at low temperature.

Samples	Lap shear strength (MPa)	Temperature (°C)
PUIP-NAGA	3.1	-50
PIL-2-TFSI	2.46	-10
P1	0.685	-18
PC$_{10}$-Water$_1$	2.49	-18
P4-AS-PAA	0.83	-20
CT-2	2.5	-20
OE	2.45	-18
PAA hydrogel	1.1	room temperature
PVA hydrogel	1.6	room temperature
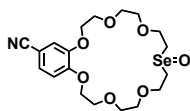
2.36   -40

C7SeO$_{10}$-H$_1$ (this work)

Table S4. The comparison of **C7SeO**$_{10}$-H$_1$ with reported supramolecular adhesives [S21] in lap shear strengths at low temperature.

References

[S1] Xu, Q.; Cui, Z.; Yao, J.; Li, B.; Lv, P.; Shen, X.; Yu, Z.; Ge, Y.; Qi, Z. Constitutionally Adaptive Crown Ether-based Macrocyclic Bolaamphiphile with Redox-responsive Switching of Lower Critical Solution Temperature Behaviors. *Chin. Chem. Lett.* **2021**, 32, 4024-4028.

[S2] a) Mathot, V.; Pyda, M.; Pijpers, T.; Van den Poel, G.; van de Kerkhof, E.; van Herwaarden, S.; van Herwaarden, F.; Leenaers, A. The Flash DSC 1, A Power Compensation Twin-type, Chip-based Fast Scanning Calorimeter (FSC): First findings on polymers. *Thermochim. Acta* **2011**, 522, 36. b) Schawe, J. E. K. J. Influence of Processing Conditions on Polymer Crystallization Measured by Fast Scanning DSC. *Therm. Anal. Calorim.* **2014**, 116, 1165.

[S3] Roy, S.; Richert, R. Dielectric Spectroscopy Study of Myoglobin in Glycerol-Water Mixtures. *Biochim. Biophys. Acta* **2014**, 1844, 323–329.

[S4] Dong, S.; Leng, J.; Feng, Y.; Liu, M.; Stackhouse, C. J.; Schönhals, A.; Chiappisi, L.; Gao, L.; Chen, W.; Shang, J.; Jin, L.; Qi, Z.; Schalley, C. A. Structural Water as an Essential Comonomer in Supramolecular Polymerization. *Sci. Adv.* **2017**, 3, eaao0900.

[S5] Abascal, J. L. F.; Vega, C. A general purpose model for the condensed phases of water: TIP4P/2005. *J. Chem. Phys.* **2005**, 123, 234505.

[S6] Wang, J.; Wolf, R. M.; Caldwell, J. W.; Kollman, P. A.; Case, D. A. Development and testing of a general amber force field. *J. Comput. Chem.* **2004**, 25, 1157-1174.

[S7] Abraham, M. J.; Murtola, T.; Schulz, R.; Páll, S.; Smith, J. C.; Hess, B.; Lindahl, E. GROMACS: High performance molecular simulations through multi-level parallelism from laptops to supercomputers. United States. https://doi.org/10.1016/j.softx.2015.06.001.

[S8] Becke, A. D. Density‐Functional Thermochemistry. I. The effect of the exchange‐only gradient correction. *J. Chem. Phys.* **1992**, 96, 2155‐2160.

[S9] Grimme, S.; Antony, J.; Ehrlich, S.; Krieg, H. A Consistent and Accurate ab initio Parametrization of Density Functional Dispersion Correction (DFT-D) for the 94 Elements H-Pu. *J. Chem. Phys.* **2010**, 132, 154104.

[S10] Gaussian 09, Revision D.01, M. J. Frisch, G. W. Trucks, H. B. Schlegel, G. E. Scuseria, M. A. Robb, J. R. Cheeseman, G. Scalmani, V. Barone, G. A. Petersson, H. Nakatsuji, X. Li, M. Caricato, A. Marenich, J. Bloino, B. G. Janesko, R. Gomperts, B. Mennucci, H. P. Hratchian, J. V. Ortiz, A. F. Izmaylov, J. L. Sonnenberg, D. Williams-Young, F. Ding, F. Lipparini, F. Egidi, J. Goings, B. Peng, A. Petrone, T. Henderson, D. Ranasinghe, V. G. Zakrzewski, J. Gao, N. Rega, G. Zheng, W. Liang, M. Hada, M. Ehara, K. Toyota, R. Fukuda, J. Hasegawa, M. Ishida, T. Nakajima, Y. Honda, O. Kitao, H. Nakai, T. Vreven, K. Throssell, J. A. Montgomery, Jr., J. E. Peralta, F. Ogliaro, M. Bearpark, J. J. Heyd, E. Brothers, K. N. Kudin, V. N. Staroverov, T. Keith, R. Kobayashi, J. Normand, K. Raghavachari, A. Rendell, J. C. Burant, S. S. Iyengar, J. Tomasi, M. Cossi, J. M. Millam, M. Klene, C. Adamo, R. Cammi, J. W. Ochterski, R. L. Martin, K. Morokuma, O. Farkas, J. B. Foresman, and D. J. Fox, Gaussian, Inc., Wallingford CT, 2016.

[S11] Emamian, S.; Lu, T.; Kruse, H.; Emamian, H. Exploring Nature and Predicting Strength of Hydrogen Bonds: A Correlation Analysis Between Atoms-in-Molecules Descriptors, Binding Energies, and Energy Components of Symmetry-Adapted Perturbation Theory. *J. Comput. Chem.* **2019**, 40, 2868–2881.

[S12] Lu, T.; Chen, F. Multiwfn: A Multifunctional Wavefunction Analyzer. *J. Comput. Chem.* **2012**, 33: 580-592.

[S13] a) Yuan, Y.; Raheja, K.; Milbrandt, N. B.; Beilharz, S.; Tene, S.; Oshabaheebwa, S.; Gurkan, U. A.; Samia, A. C. S.; Karayilan, M. Thermoresponsive Polymers with LCST Transition: Synthesis, Characterization, and Their Impact on Biomedical Frontiers. *RSC Appl. Polym.* **2023**, 1, 158-189. b) Lemanowicz, M.; Gierczycki, A.; Kuźnik, W.; Sancewicz, R.; Imiela, P. Determination of Lower Critical Solution Temperature of Thermosensitive Flocculants. *Miner. Eng.* **2014**, 69, 170-176. c) Foster, J. C.; Akar, I.; Grocott, M. C.; Pearce, A. K.; Mathers, R. T.; O'Reilly, R. K. 100th Anniversary of Macromolecular Science Viewpoint: The Role of Hydrophobicity in Polymer Phenomena. *ACS Macro Lett.* **2020**, 9, 1700-1707.

[S14] Kremer, F.;, Różańki, S. A. The Dielectric Properties of Semiconducting Disordered

Materials In F. Kremer, A. Schönhals (Eds) Broadband Dielectric Spectroscopy, Springer, **2003**.

[S15] Jonscher, A. K. The 'Universal' Dielectric Response. *Nature* **1977**, 267 (5613), 673–679.

[S16] Kobayashi, M.; Tanaka, H. The Reversibility and First-order Nature of Liquid–Liquid Transition in a Molecular Liquid. *Nat. Commun.* **2016**, 7, 13438.

[S17] a) Vogel, H. Das Temperaturabhänigkeitsgesetzt der Viskosität von Flüssigkeiten. *Phys. Z.* **1921**, 22, 645. b) Fulcher, G. Analysis of Recent Measurements of The Viscosity of Glasses. *J. Am. Ceram. Soc.* **1925**, 8, 339. c) Tammann, G.; Hesse, W. Die Abhängigkeit der Viskosität von der Temperatur bei unterkühlten Flüssigkeiten. *Anorg. Allg. Chem.* **1926**, 156, 245.

[S18] Tang, C. G.; Syafiqah, M. N.; Koh, QM.; Ang, M. CY.; Choo, KK.; Sun, MM.; Callsen, M.; Feng, YP.; Chua, LL.; Png, RQ.; Ho, P. K. H. Water Binding and Hygroscopicity in π-conjugated Polyelectrolytes. *Nat. Commun.* **2023**, 14, 3978.

[S19] Chen, HC.; Lin, HC.; Chen, HH.; Mai, FD.; Liu, YC.; Lin, CM.; Chang, CC.; Tsai, HY.; Yang, CP. Innovative Strategy with Potential to Increase Hemodialysis Efficiency and Safety. *Sci. Rep.* **2014**, 4, 4425.

[S20] a) Baba, T.; Sakamoto, R.; Shibukawa, M.; Oguma, K. Solute Retention and the States of Water in Polyethylene Glycol and Poly(vinyl alcohol) Gels. *J. Chromatogr. A* **2004**, 1040, 45−51. b) Prawitwong, P.; Takigami, S.; Phillips, G. O. Phase Transition Behaviour of Sorbed Water in Konjac Mannan. *Food Hydrocolloids* **2007**, 21, 1368−1373.

[S21] a) Yao, Y.; Xu, Z.; Liu, B.; Xiao, M.; Yang, J.; Liu, W. Multiple H-Bonding Chain Extender-Based Ultrastiff Thermoplastic Polyurethanes with Autonomous Self-Healability, Solvent-Free Adhesiveness, and AIE Fluorescence. *Adv. Funct. Mater.* **2021**, 31, 2006944. b) Zhang, J.; Chen, Z.; Zhang, Y.; Dong, S.; Chen, Y.; Zhang, S. Poly(ionic liquid)s Containing Alkoxy Chains and Bis(trifluoromethanesulfonyl)imide Anions as Highly Adhesive Materials. *Adv. Mater.* **2021**, 33, 2100962. c) Li, X.; Deng, Y.; Lai, J.; Zhao, G.; Dong, S. Tough, Long-Term, Water-Resistant, and Underwater Adhesion of Low-Molecular-Weight Supramolecular Adhesives. *J. Am. Chem. Soc.* **2020**, 142, 5371-5379. d) Li, X.; Lai, J.; Deng, Y.; Song, J.; Zhao, G.; Dong, S. Supramolecular Adhesion at Extremely Low Temperatures: A Combined Experimental and Theoretical Investigation. *J. Am. Chem. Soc.* **2020**, 142, 21522-21529. e) Cui, C.; Gu, R.; Wu, T.; Yuan, Z.; Fan, C.; Yao, Y.; Xu, Z.; Liu, B.; Huang, J.; Liu, W. Zwitterion-Initiated Spontaneously

Polymerized Super Adhesive Showing Real-Time Deployable and Long-Term High-Strength Adhesion against Various Harsh Environments. *Adv. Funct. Mater.* **2022**, 32, 2109144. f) Wu, S.; Cai, C.; Li, F.; Tan, Z.; Dong, S. Supramolecular Adhesive Materials from Natural Acids and Sugars with Tough and Organic Solvent-Resistant Adhesion. *CCS Chem.* **2021**, 3, 1690-1700. g) Wu, S.; Wang, W.; Cai, C.; Li, F.; Dong, S. Low-molecular-weight supramolecular adhesive with resistance to low temperatures. *Chin. Chem. Lett.* **2023**, 34, 107830. f) Li, X.; Wang, Z.; Li, W.; Sun, J. Superstrong Water-Based Supramolecular Adhesives Derived from Poly(vinyl alcohol)/Poly(acrylic acid) Complexes. *ACS Mater. Lett.* **2021**, 3, 875-882.